JOURNAL OF COMPUTATIONAL PHYSICS 114, 234–256 (1994)

Optimisation Methods for Bathymetry and Open Boundary Conditions in a Finite Element Model of Ocean Tides

F. LYARD AND M. L. GENCO

Equipe de Modélisation des Ecoulements Océaniques et des Marées Laboratoire des Ecoulements Géophysiques et Industriels-Institut de Mécanique de Grenoble, BP 53X, 38 041 Grenoble, France

Received April 12, 1993; revised February 24, 1994

A bidimensional, spectral in time, quasi-linearised hydrodynamic ocean tide model has been developed at the Institut de Mécanique de Grenoble. This model is derived from the classical shallow water equations by removing velocity unknowns in the continuity equation, that leads to an elliptic, second-order differential equation where tide denivellation remains the only unknown quantity. The problem is solved in its variational formulation and the finite elements method is used to discretise the equations in the spatial domain with a Lagrange-P2 approximation. Bottom topography has to be known at the integration points of the elements. In the case of the large oceanic basins, a specific method, called the bathymetry optimisation method, is needed to correctly take into account the bottom topography inside the model. The accuracy of the model's solutions is also strongly dependent on the quality of the open boundary conditions because of the elliptic characteristics of the problem. The optimisation method for open boundary conditions relies on the use of the *in situ* data available in the modelled domain. The aim of this paper is to present the basis of these optimisations of bathymetry and open boundary conditions. An illustration of the related improvements is presented on the North Atlantic Basin.

1. INTRODUCTION

In the already very advanced field of knowledge of oceanic tides, demands for accuracy have risen notably over these past few years, particularly because of the needs of altimetric satellite surveying of the sea surface. The tidal signal must be removed from the altimetric signal in order to give access to the so-called oceanic signal, which is the surface's real signature of the ocean's large and meso scale circulations. The accuracy required to make this correction had not been attained by the mid eighties with the existing world tidal models [1], hence there has been renewed interest in this field in recent years. Among this new work, an original hydrodynamic model, formulated by Le Provost and Poncet [2] in 1978 and first applied to coastal tides (cf. Le Provost *et al.* [3]), has been extended to oceanic tides (cf. Vincent and Le Provost [4]). This model has recently been adapted to the resolution of tidal waves on a planetary scale with the objective of improving the existing overall solutions (i.e., Schwiderski [5, 6]], noted NSWC, and Cartwright and Ray [7], noted CR), which are usually considered as the best available solutions on the world ocean at the moment (in terms of spatial resolution and level of accuracy when comparing with tidal observations). The first applications to regional basins (cf. Vincent and Le Provost [4]) have shown the ability of the model to represent the tidal dynamics correctly both in oceanic and coastal regions and provided a validation of its formulation by the high level of precision of its solutions. This model has been applied to the large oceanic basins (by Genco [8] in the North and South Atlantic, Lyard [9] in the Indian Ocean, and Canceill [10] in the Pacific Ocean) with an optimal resolution in order to provide accurate tidal charts on the World Ocean. As a first step, the model was simply extended to planetary basins, without any change in the modelling procedures, described by Le Provost and Vincent [11]. However, the tidal solutions obtained in this way, although better over shelf or coastal regions, were generally of the same level of accuracy as the NSWC or CR models in deep ocean areas. These results could already have been considered satisfactory, but the authors were convinced that better results were attainable, particularly in view of the preliminary results previously obtained in regional applications. Because of the loss of precision, possible causes of model deteriorations were sought in the numerical and input data fields. The performance of finite element models based on the wave continuity equation have already been studied by many authors (see for example, Lynch [12] and Kolar *et al.* [13]). Two specific points were finally identified as being the main sources of the problems observed. The first point is the discretisation error in the integral terms of the variational formulation of the model. The necessary spatial resolution in shelf and coastal regions leads to major linear systems which may be very sensitive to the propagation of numerical and discretisation errors (the meaning of these two terms will be defined precisely in the second sec-

0021-9991/94 $6.00

tion). The second point concerns the strong dependence of the accuracy of the solutions on the quality of the conditions prescribed at the open boundaries. Moreover, the discrepancy between the conditions and truth can be amplified inside the modelling domain. This dependence is due to the elliptic characteristic of the model. Nevertheless, because of the lack of *in situ* oceanic observations along the open basin limits, boundary conditions have to be drawn from existing overall or regional models which obviously are not perfect.

The purpose of this paper is to describe the improvements introduced into the model of Le Provost and Vincent [11] enabling the production of more precise tidal solutions on an overall scale. In the first section a technique is presented for minimising the discretisation error by adjusting the discrete description of the bottom topography used in the model. A set of criteria that permit the definition of a numerically optimal model bathymetry is proposed. In the second part, an open boundary condition optimisation method is described. This method is similar to an optimal control [14] using a first solution as the reference and a set of available *in situ* data inside the domain. Optimised open boundary conditions are obtained by solving a least-squares problem, minimising the discrepancy between the solution and the observations. A new solution can then be obtained by solving the direct problem using the newly found optimised boundary conditions. In the third part of the paper, modelling of the M_2 tide on the North Atlantic Basin is used as an illustration of the gain in precision that can be expected by using these two methods.

1. THE MODEL

The basic characteristics of our hydrodynamic model are presented here. In order to simplify the presentation, notation definitions and model equations have been moved to Appendices I and II and Fig. 1. The basic equations used in barotropic tidal motion models are the classic non-linear, depth-averaged shallow water equations in geocentric coordinates. Forcing includes astronomical sun and moon potential, plus loading and self-attraction effects. Bottom friction is taken into account by a Chezy-like law, while the internal friction is ignored. In order to avoid numeric instability (cf. Lynch [15]) and to reduce the number of unknowns, velocity is removed from the continuity equation by using a quasi linearisation of momentum equations that leads to an elliptic, second-order differential equation, called the wave continuity equation [16], where the tidal elevation remains the only unknown quantity to be computed (the hydrodynamic equations are detailed in Appendix II). The variational formulation of the problem is discretised in the spatial domain by the finite element method, using a triangular mesh associated with a Lagrange-P2 approximation (the discrete model equations are detailed in Appendix II). The finite element method was chosen because of the elliptic nature of Eq. (32) and the need for a variable spatial resolution to adapt the mesh size in a consistent way to the local wavelength (the wavelength of a tidal wave can be expressed by $\Lambda = (2\pi/\omega)\sqrt{gH}$). The model mesh is automatically built by the mesh generator TRIGRID [17] which can be constrained by the bathymetry. The typical resolution at the closed boundaries is about 15 km between two nodes, making it possible to take into account the smaller tidal wavelength on continental shelves, where most dissipation of the tidal energy takes place. The spatial resolution increases to about 200 km in the deep ocean. Discretisation of the large oceanic basins leads to meshes which contain roughly 15000 elements (i.e., 30000 complex unknowns in the Lagrange-P2 approximation).

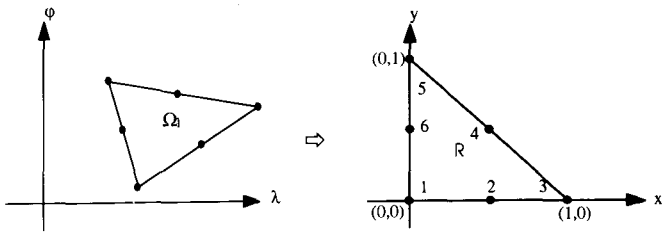

FIG. 1. Affine transform T_1 from a real world element Ω_1 to the reference element R for the Lagrange-P2 approximation. The ith node of R is the image of the real world node n which appears in ith position of the anticlockwise description of Ω_1.

2. OPTIMISATION OF MODEL BATHYMETRY

Over continental shelves and in the deep ocean, tidal wavelengths vary from a few hundred kilometres to a few thousand and more. For that reason, it is generally admitted that tidal waves are not sensitive to the small wavelengths of the bottom topography. So the most usual technique for obtaining model bathymetry from data consists in smoothing the original topographic data field by a Gaussian function. A similar procedure was used in the first applications of the model (Le Provost *et al.* [3]). In fact, an experiment has shown that this credo has to be reconsidered, particularly when the number of nodes in the model mesh increases to great values. This experiment involved slightly modifying the smoothing definition. The consequence was surprising changes in solutions, even in the deep ocean where differences between the two model bathymetries were apparently insignificant. The reason for this is that the way the bathymetry is taken into account in the matrix S coefficients contribute to the error budget of the discretisation of the variational equation. Let us examine a typical term of the integral Eq. (42):

$$J^l_{A,m,n} = \iint_{\Omega_l} A(\lambda, \varphi) \cos\varphi \frac{\partial P_{i(m,l)}}{\partial \varphi} \frac{\partial P_{i(n,l)}}{\partial \varphi} d\lambda\, d\varphi.$$

Its numerical approximation by the Hammer formula gives

$$\tilde{J}^{l}_{A,m,n} = \text{Jacobian}(T_l) \times \sum_{k=1}^{NPG} p_k A(\lambda_k, \varphi_k) \times \cos\varphi_k \left.\frac{\partial P_{\iota(m,l)}}{\partial \varphi}\right|_{(\lambda_k,\varphi_k)} \left.\frac{\partial P_{\iota(n,l)}}{\partial \varphi}\right|_{(\lambda_k,\varphi_k)}.$$

The error due to the use of the Hammer formula is referred to as the integration error. The error due to the discretisation of A when computing its value at the integration points is referred to as the discretisation error. Estimation of the discretisation and integration errors, i.e., $\varepsilon_{l,m,n} = J_{l,m,n} - \tilde{J}_{l,m,n}M$ depends on the complexity in space of the term A, and, hence on the complexity in space of the bottom topography. It is not the aim of this paper to carry out a full numerical study on numerical integration. But the term A has some natural properties which enable that error to be cancelled almost everywhere by using a particular model bathymetry.

In order to simplify the presentation, the statement is restricted to the case of the dominant wave. It would be analogous in the case of any other wave. Bottom friction terms related to the dominant wave are:

$$r = r''' = \frac{C_f}{H}R, \qquad r' = -r'' = j\frac{C_f}{H}R'. \tag{1}$$

Replacing the coefficients r'', r''' in the A expression yields

$$A = \frac{gH}{a^2} \times \frac{(r + j\omega)}{(\omega^2 - f^2 + 2fr' - r'^2 - r^2 - 2j\omega r)}. \tag{2}$$

The value of r, r' can be estimated from Eq. (22), Eq. (23), and Eq. (24):

$$|r| = O\left(\frac{C_f}{H}\|u\|\right), \qquad |r'| = O\left(\frac{C_f}{H}\|u\|\right). \tag{3}$$

Typical size scales for terms appearing in the expression of A are summarised in Table II, where deep ocean plus shelf regions and coastal regions are distinguished because of the great variation in bathymetry, velocity, and dissipation scales between both cases. Dissipation terms vanish in the deep ocean, and remain of a much lower order than frequency and the Coriolis parameter over shelves, except in a very thin zonal band corresponding to the critical latitude of the wave. On the other hand, however, they may sometimes be of the same order as the wave frequency or the local inertial frequency over coastal regions. Disregarding coastal regions and the critical latitude band, which represent a minor part of the total modelling domain area, it may be assumed that

$$r, r' \ll \omega, f, \qquad j\omega r - fr' \ll \omega^2 - f^2, \qquad r^2 + r'^2 \ll \omega^2 - f^2. \tag{4}$$

The term A can thus be approximated almost everywhere by the serial development:

$$A \approx \frac{gH}{a^2}\frac{jw}{\omega^2 - f^2}\left[1 - \frac{jr}{\omega}\right] \times \left[1 + 2\frac{(j\omega r - fr')}{\omega^2 - f^2} + 2\left(\frac{j\omega r - fr'}{\omega^2 - f^2}\right)^2 + \frac{r'^2 + r^2}{\omega^2 - f^2}\right]. \tag{5}$$

Removing terms of a greater order than two in Eq. (5) yields

$$A \approx \frac{gH}{a^2}\frac{j\omega}{\omega^2 - f^2}\left[1 \underbrace{- \frac{jr}{\omega} + \frac{2(j\omega r - fr')}{\omega^2 - f^2}}_{O(r/\omega)} \underbrace{- \frac{jr}{\omega}\frac{2(j\omega r - fr')}{\omega^2 - f^2} + 2\left(\frac{j\omega r - fr'}{\omega^2 - f^2}\right)^2 + \frac{r'^2 + r^2}{\omega^2 - f^2}}_{O(r^2/\omega^2)}\right].$$

Using the relation Eq. (1), A can be written

$$A \approx \frac{g}{a^2}\frac{j\omega}{\omega^2 - f^2}\left[H + c_0 L + c_1 L^2 \frac{1}{H}\right] = A_1 + A_0 + A_{-1}, \tag{6}$$

where $L = C_f\|u\|/\omega < 1$, $c_0 = O(1)$, $c_1 = O(1)$. Thus discretisation of the bathymetry is crucial for discretisation of A. The difficulty of discretising the bottom topography in a way that is consistent with the model comes from its high variability in the space aspect and this is the reason why smoothing procedures, which filter the small spatial scales, are usually used. But it is not easy to estimate the consistency of the filtering, as the tidal wavelength also varies with the depth, making it necessary to adapt the filter to local depths. Now let us suppose that the exact bathymetric field H is known all over the domain. Let $\hat{h}$ be the bathymetric field defined in a such way that its values at the integration points coincide with the depths given to the model (i.e., h is the extension to the whole element of the depth given at the integration points). This field, called the image field, as it is the image of the real world through the discretisation procedure, is rarely computed exhaustively, but it is practical here to consider the image field $\hat{h}$ as a discretisation of H and the values computed at the integration points as an interpolation of the image field. Then the question is "what is an image field able to transmit

consistent bathymetric information to the model through numerical integration?" Let us examine the first-order term as it is integrated (it is assumed here that the term $\cos\varphi/(\omega^2 - f^2)$ is constant over an element):

$$I_1 = \iint_{\Omega_l} A_l \cos\varphi \frac{\partial\beta_m}{\partial\varphi}\frac{\partial\beta_n}{\partial\varphi}\,d\lambda\,d\varphi$$

$$= \text{Jacobian}(T_l)\, j \frac{g\omega}{a^2}\frac{\cos\varphi_0}{\omega^2 - f^2}$$

$$\times \iint_R \left[H \frac{\partial P_{\iota(m,l)}}{\partial\varphi}\frac{\partial P_{\iota(n,l)}}{\partial\varphi}\right](x, y)\,dx\,dy.$$

Cancelling the discretisation and numerical integration errors leads to the following two conditions, which have to be respected by the model bathymetry $\hat{h}$,

$$\iint_R \hat{h}(x, y)\, Q(x, y)\,dx\,dy$$

$$= \sum_{\text{NPG}} p_k \hat{h}(x_k, y_k)\, Q(x_k, y_k) \qquad (7)$$

$$\iint_R H(x, y)\, Q(x, y)\,dx\,dy$$

$$= \iint_R \hat{h}(x, y)\, Q(x, y)\,dx\,dy$$

$$\forall Q \text{ polynomial of degree } n, \qquad (8)$$

where n is equal to twice the degree of the derivative of the basis interpolation polynomials, i.e. 0 in the case of a Lagrange-P1 approximation, 2 in the case of a Lagrange-P2 approximation. An image field obtained by a smoothing method is almost satisfactory in the meaning of Eq. (7), when it is smooth enough, but it is not visibly satisfactory in the meaning of Eq. (8). On the other hand, an image field satisfying both Eq. (7) and Eq. (8) can be sought, for each element of the mesh, in the polynomial space, with the additional criterion that the degree of the solution should be as low as possible, i.e., n itself. Eq. (8) is equivalent to $(n+1)(n+2)/2$ relations that can be summarised by:

$$\iint_R H(x, y)\, x^k y^l\,dx\,dy = \iint_R \hat{h}(x, y)\, x^k y^l\,dx\,dy, \qquad k + l \leqslant n. \qquad (9)$$

With respect to Eq. (9), an optimal approximation of the bathymetry in the case of the Lagrange-P1 approximation is the constant value equal to a 'mean' depth over the element defined by:

$$\hat{h}|_{\Omega_l}(\lambda, \varphi) = \hat{h}(x, y) = cste = \frac{\iint_R H(x, y)\,\partial x\,\partial y}{\iint_R \partial x\,\partial y},$$

$$\text{where} \quad (\lambda, \varphi) \xrightarrow{T_l} (x, y).$$

In the case of the P1 approximation, it may be noted that a model bathymetry obtained by a smoothing procedure, which maintains the mean values, almost satisfies Eq. (9) and that Eq. (7) is verified by using a Hammer formula based on one Gauss point. That definition is similar to the one proposed by Platzman [18]. In the case of the Lagrange-P2 approximation, for each element of the mesh, a polynomial approximation of degree 2 of the bathymetry which respects the momentum of an order equal to or lower than 2 of the "real" bathymetry can be computed from Eq. (9). The model bathymetry can be expressed on the basis of the P2-Lagrange polynomials:

$$\hat{h}|_{\Omega_l}(\lambda, \varphi) = \hat{h}(x, y) = \sum_{i=1}^{6} \hat{h}_i (P_i \circ T_l)(\lambda, \varphi),$$

$$\text{where} \quad (\lambda, \varphi) \xrightarrow{T_l} (x, y).$$

Equation (7) is verified by using a Hammer formula based on seven Gauss points (see Table I). The model bathymetry thus obtained is continuous inside an element, but it is not automatically at the limit between two elements, because the $\hat{h}_i$ coefficients are computed separately for each element. This does not present any particular problem unless the bathymetry has to be known at the nodes of the grid for a specific use. This difficulty can be partially eliminated by seeking the nearest bathymetry defined at the nodes, using a least-square method.

Integration of the second term, corresponding to A_0 in Eq. (6), does not present any particular problem because it varies like the norm of the velocity, which is almost linear over the triangle when using the P2-Lagrange approximation. So Hammer's numerical approximation is satisfactory for the second term as well as for the first term. No particular conclusion was reached about the effect of using a model bathymetry defined by Eq. (9) on the precision of third term integration, as this question was not investigated on the assumption that its amplitude is much smaller than that of term A_1 and A_0 almost everywhere. It may be possible to perform a similar study in order to improve the model in regions where the basic assumption (i.e., Eq. (4))

TABLE I

Relation between the Number of Gauss Points in Hammer's Numerical Integration Method and the Maximum Degree m of the Exactly Integrated Polynomials

Amount of Gauss points NPG	Total degree m
3	2
6	4
7	5
12	6
16	7

is no longer relevant. But, in addition to the fact that the effects would be very local, the consistency of the model bathymetry is not the major component of the model's error budget in the shallower areas. Actually, controlling discretisation error by bathymetry terms can work efficiently only if the real bathymetry field is well known and it is now recognised that the data bank ETOPO5 [19], from which the bathymetry is drawn, is of very poor quality in very shallow spots such as on shore regions, although it is at present the best unclassified data set that civilians can use.

In conclusion, minimisation of integration and discretisation errors almost everywhere can be carried out by adjusting model bathymetry. Moreover, this study has indicated what bathymetric information is crucial to a finite element model when using a variational formulation. The model bathymetry must respect the average value of the bottom topography over each element in the case of a P1 approximation, and the momentum of an order equal to or lower than 2 of the bottom topography over each element in the case of a P2 approximation.

3. BOUNDARY CONDITION OPTIMISATION

4.1. *Theoretical Approach: Introduction to the Least-Square Problem*

The validation of numerical models is usually based on a comparison of the solution with *in situ* observations which give local information on the accuracy of the solutions. An overall estimate of the model's quality is more difficult to achieve because it is not possible to define an absolute criterion. However, an assessment may be made by computing the RMS of the discrepancies between solutions and data on a representative set of control stations. In the following, the terms of accuracy and quality will be referred to that criterion. The elliptic shape of the model implies that the inner quality of the solutions is strongly dependent on the quality of the prescribed open boundary conditions. Thus determination of the boundary conditions is a critical point of the modelling strategy. The easiest way to prescribe the value of the solution on open boundaries is, of course, to possess *in situ* data along the limits. Unfortunately, it is usually not possible to choose the domain limits so that they will coincide with a chain of regularly sampled observation sites which could be used for obtaining boundary conditions. In such cases, an alternative strategy must be defined, which involves setting the domain limits inside areas where preexisting tidal models are available. Because of the uncertainty concerning the quality of such tidal models, these limits have to be set outside the critical areas where prescribing a value is known to amplify the model's sensitivity to boundary condition errors, such as the vicinity of amphidromic points, and inside regions where the preexisting models are known to be of reasonable accuracy. In the case of a lack of accurate regional models, such as Flather's model in the North East Atlantic [20], the overall solutions NSWC or CR have to be used; thus the performance of a new model is at least limited by the quality of these solutions. As can be expected by considering the elliptic shape of the problem, some sensitivity tests have shown that errors due to boundary conditions are propagated and sometimes amplified far inside the modelling domain. Because the aim of the present model is to improve previous knowledge, it is necessary to improve that input parameter. Discretisation of the variational equation leads to a linear system, which can be written:

N: number of nodes in the domain

N_b: number of open boundary nodes

N_d: number of observations

N_n: number of nodes needed to interpolate the solution at the observation stations

$S\alpha = F$, where

$S = [s_{i,j}]$: linear system $N \times N$ complex matrix

$\alpha = [\alpha_i]$: elevation N rows complex vector

$F = [f_i]$: forcing N rows complex vector

In order to take into account the open ocean boundary conditions, rows corresponding to open boundary nodes are transformed before the resolution of the linear system so that:

$$\left.\begin{aligned} s_{ij} &= \delta_{ij} \\ f_i &= \alpha_i^0 \end{aligned}\right\} \quad \text{if node } i \text{ belongs to } \Gamma_2, \text{ where } \delta_{ij}$$

represent the Kronecker symbols.

Considering the "cost" function defined by the variance of the discrepancies computed between a reference solution and a set of observations:

ξ_i^d: observation at station No. i

ξ_i: interpolation of the solution α at station No. i

$$J(0) = \frac{1}{N} \sum_{\text{observations}} |\xi_i^d - \xi_i|^2 = \frac{1}{N} \sum_{\text{observations}} |e_i|^2.$$

Considering T the finite element interpolation matrix: $T\alpha = \zeta$, where

$\zeta = [\zeta_i]$: N_d rows complex vector

$T = [t_{i,j}]$: $N_d \times N$ matrix with $t_{i,j} = \beta_j(\lambda_i, \varphi_i)$

Perturbing the boundary conditions around the reference condition leads to a new solution, which can be written as the sum of the reference solution plus a perturbation $\delta\alpha$. This perturbation is explicitly defined by

$$\delta\alpha = S^{-1}\,\delta F \qquad \text{with} \quad \begin{cases} \delta F_i = 0, & i \notin \Gamma_2 \\ \delta F_i = \delta\alpha_i^0, & i \in \Gamma_2. \end{cases}$$

The corresponding cost function is defined by

$$J(\delta\alpha^0) = \frac{1}{N} \sum_{\text{observations}} |\xi_i^d - \xi_i - \delta\xi_i|^2$$

$$= \frac{1}{N} \sum_{\text{observations}} |e_i - \delta\xi_i|^2.$$

The gradient of a scalar quantity J with respect to a complex value u is defined by

$$\nabla_u J = \frac{\partial J}{\partial u^r} + i \frac{\partial J}{\partial u^i}, \qquad \text{where } u^r \text{ and } u^i \text{ are respectively the real and imaginary parts of } u. \tag{10}$$

The solution of the least square problem is the perturbation such that

$$\nabla_{\delta\alpha^0} J(\delta\alpha^0) = 0.$$

Considering a system where u is an input vector and v is an output vector, the gradient of a scalar quantity J with respect to u can be linked to the gradient of J with respect to v:

$$v = M(u)$$

$$\delta v = M' \, \delta u, \qquad \text{where } M' \text{ is the Jacobian of } M$$

$$\nabla_u J = M'^* \, \nabla_v J, \qquad \text{where } M'^* \text{ is the adjoint matrix of } M'.$$

In the linear case, this relation is simplified by

$$v = Mu$$

$$\nabla_u J = M^* \, \nabla_v J \text{ where } M^* \text{ is the adjoint matrix of } M. \tag{11}$$

As M is a complex-valued matrix, the adjoint matrix of M is the transposed conjugate matrix of M. Applying Eq. (11) to the gradient of the cost function yields

$$\nabla_{\delta\alpha^0} J(\delta\alpha^0) = (S^{-1})^* \, \nabla_{\delta\alpha} J(\delta\alpha^0) = -2(S^{-1})^* \, T^*(e - \delta\xi).$$

Finally the least square problem can be expressed by

$$\nabla_{\delta\alpha^0} J(\varepsilon) = 0 \Leftrightarrow (TS^{-1})^* \, (TS^{-1})[\varepsilon_i] = (S^{-1})^* \, T^*[e_i], \tag{12}$$

where

$$\varepsilon \equiv \delta F \text{ with } \begin{cases} \varepsilon_i = 0, & \text{if the node } i \text{ is an inner node} \\ \varepsilon_i = \delta\alpha_i^0, & \text{if the node } i \text{ is an open boundary node.} \end{cases}$$

4.2. *Theoretical Approach: The Regularised Least-Square Problem*

In practical applications, many situations have been encountered where the data are not sufficient to obtain an acceptable solution of the least square problem defined by Eq. (12). Some numerical tests have shown that the perturbations of the boundary conditions may attain some unrealistic values in terms of magnitude and gradients, when the decrease in the misfits is of only a few centimetres. The question of data sufficiency has already been discussed in the assimilation literature (see for example Thacker and Long, [21]). Briefly, some possible causes of troubles should be pointed out. First, the total amount of available data is most of the time much lower than the total number of open boundary nodes. Moreover, the spatial distribution is generally heterogeneous, and the dependency of the solution at the data points with respect to certain boundary conditions may be weak. The presence of corrupted data or model deficiencies can also affect the method. Thus the least square method may produce unacceptable results. To avoid this, a term must be added to minimise the boundary condition pertubations, in addition to the original formulation. It may also be necessary to parametrise the perturbation in order to reduce the number of unknowns in the least square problem. A set of parameters is defined for each limit of the domain and the perturbations are defined by

$$\delta\alpha^0(s) = \sum_K a_k f_k(s),$$

K is the number of parameters, where s is the curvilinear abscissa along the open boundaries, f_k are analytic functions of s, and a_k are the new unknowns of the least square problem. The shape of the parametrisation must be as consistent as possible with the tidal hydrodynamics. One possible shape is

$$\delta\alpha^0(s) = a_{k,0} + a_{k,1} x + \sum_{n=1}^{N_1} (b_{k,n} e^{-2^n x/L_1}) + \sum_{n=1}^{N_2} (c_{k,n} e^{-2^n(1-x)/L_2}),$$

where

L_1, L_2: typical horizontal scales,

$\tilde{s}$: limit segment length,

x: dimensionless parameter,

N_1, N_2: number of wavelengths used,

$$x = s/\tilde{s}_k, \qquad 2^N L \leqslant \tilde{s}_k \leqslant 2^{n+1} L.$$

This formulation refers to the exponential dependence in space of the simpler long gravity wave solution for a basin on a rotating sphere, i.e., a Kelvin wave. The characteristic lengths L_1 and L_2 can be related to the external deformation radius R_d,

$$R_d = c/f \qquad \text{with } c, \text{ the wave's celerity, } c = \sqrt{gH}.$$

Experience shows that it is necessary to include the perturbation minimisation condition even in the case of parameterised perturbations. Furthermore, it makes sense to introduce a second derivative minimisation condition to avoid large variations in the perturbation gradient. The summation is weighted to modulate the influence of the different terms, making the new coast function:

$$J(\boldsymbol{\varepsilon}) = \sum_{\text{observations}} p_i^2 \, |e_i - \delta\xi_i(\boldsymbol{\varepsilon})|^2 + \int_{\Gamma_2} q^2(s) \, |\delta\alpha^0(s)|^2 \, ds + \int_{\Gamma_2} w^2(s) \, |\delta\alpha^{0''}(s)|^2 \, ds \tag{13}$$

where $\delta\alpha^{0''} = \partial^2\delta\alpha^0/\partial s^2$ is the second derivative of $\delta\alpha^0$ along the open limits.

The positive coefficients p and q are weights related to the *a priori* trust given to the corresponding quantities. As the second derivative term reflects the correlation between the perturbations themselves, the positive coefficient w is related to the variability of the tidal dynamic along the open boundaries. In the case of parameterised perturbations, the dynamic already appears in the shape of the parametrisation and the weight w can possibly be set to zero. As the optimisation procedure presented in this paper (see below) was applied using nonparameterised perturbations and, in order to simplify the presentation, only this case will be detailed in the following:

$$\begin{aligned} J_1 &= \sum_{\text{observations}} p_i^2 \, |e_i - \delta\xi_i(\boldsymbol{\varepsilon})|^2 \\ \nabla_{\boldsymbol{\varepsilon}} J_1 &= (TS^{-1})^* \, \nabla_{\delta\xi} J_1 = 2(TS^{-1})^* \, M^p(\delta\xi - \mathbf{e}), \end{aligned} \tag{14}$$

where $M^p = [p_i^2 \delta_{ij}]$ and M^p is a diagonal matrix. The physical interpretation of this particular shape is that the observation errors are assumed to be uncorrelated; we have

$$J_2 = \int_{\Gamma_2} q^2(s) \, |\varepsilon|^2 \, ds = \int_{\Gamma_2} \left| \sum_N q_n \varepsilon_n \beta_n(s) \right|^2 ds = \sum_{m,n} q_m q_n \bar{\varepsilon}_m \varepsilon_n \int_{\Gamma_2} \beta_m(s) \, \beta_n(s) \, ds,$$

defining the symmetrical coefficients

$$\int_{\Gamma_2} \beta_m(s) \, \beta_n(s) \, ds = B_{m,n}.$$

Developing J_2 yields

$$\begin{aligned} J_2 &= \sum_n q_n^2 B_{n,n} \, |\varepsilon_n|^2 + \sum_{m<n} q_m q_n B_{m,n} (\bar{\varepsilon}_m \varepsilon_n + \varepsilon_n \bar{\varepsilon}_n) \\ &= \sum_n q_n^2 B_{n,n} \, |\varepsilon_n|^2 + \sum_{m<n} 2 q_m q_n B_{m,n} (\varepsilon_m^r \varepsilon_n^r + \varepsilon_m^i \varepsilon_n^i). \end{aligned} \tag{15}$$

The gradient of J_2 with respect to the kth component of the boundary condition perturbation can be developed by using the relation Eq. (10),

$$\nabla_{\varepsilon_k} J_2 = 2q_k^2 B_{k,k} \varepsilon_k + \sum_{m \neq k} 2 q_m q_k B_{m,k} \varepsilon_m = 2 \sum_m q_m q_k B_{m,k} \varepsilon_m,$$

giving the gradient of J_2 with respect to the perturbation vector in matrix notation

$$\nabla_{\boldsymbol{\varepsilon}} J_2 = 2M^{q'} \boldsymbol{\varepsilon} \qquad \text{where} \quad M^{q'} = [m_{i,j}^{q'}] = [q_i q_j B_{i,j}].$$

In the case of a non-parameterised perturbation, the derivative is replaced by the finite difference discretisation:

$$(\varepsilon)'_{j-1/2} = \frac{\varepsilon_j - \varepsilon_{j-1}}{s_j - s_{j-1}}, \qquad (\varepsilon)'_{j+1/2} = \frac{\varepsilon_{j+1} - \varepsilon_j}{s_{j+1} - s_j}.$$

The second-order derivative can be calculated approximately by the discrete formula

$$(\varepsilon)''_j = \frac{(\varepsilon)'_{j+1/2} - (\varepsilon)_{j-1/2}}{s_{j+1/2} - s_{j-1/2}} = \kappa_1 \varepsilon_{j-1} + \kappa_2 \varepsilon_j + \kappa_3 \varepsilon_{j+1}$$

in matrix notation:

$$\begin{aligned} &[\varepsilon''] = C[\varepsilon], \\ &c_{j,j-1} = \kappa_1, \qquad c_{j,j} = \kappa_2, \qquad c_{j,j+1} = \kappa_3, \\ &c_{j,k} = 0 \qquad \text{if} \quad k \notin \{j-1, j, j+1\}. \end{aligned}$$

The third term of J can be developed in the same way as J_2:

$$J_3 = \int_{\Gamma_2} w^2(s) \, |\varepsilon''|^2 \, ds = \int_{\Gamma_2} \left| \sum_N w_n \varepsilon_n'' \beta_n(s) \right|^2 ds = \sum_{m,n} w_m w_n B_{m,n} \bar{\varepsilon}_m'' \varepsilon_n''. \tag{16}$$

Using relation Eq. (10) gives the gradient of J_3 with respect to the perturbation vector in matrix notation $\nabla_{\boldsymbol{\varepsilon}} J_3 = C^* \nabla_{\boldsymbol{\varepsilon}''} J_3 = 2C^* M^{w'} \boldsymbol{\varepsilon}'' = 2C^* M^{w'} C\boldsymbol{\varepsilon}$, where $M^{w'} = [m_{i,j}^{w'}] = [w_i w_j B_{i,j}]$. Finally, $\frac{1}{2}\nabla_{\boldsymbol{\varepsilon}} J(\boldsymbol{\varepsilon}) = (TS^{-1})^* \, M^p(\delta\xi - \mathbf{e}) + M^{q'}\boldsymbol{\varepsilon} + C^* M^{w'} \boldsymbol{\varepsilon}''$. The optimal boundary condition perturbation is then the solution of the linear system,

$$\begin{aligned} \nabla_{\boldsymbol{\varepsilon}} J = 0 \Leftrightarrow &[(S^{-1})^* \, T^* M^p T(S^{-1}) + M^{q'} + C^* M^{w'} C][\varepsilon_i] \\ &= (S^{-1})^* \, T^* M^p [e_i]. \end{aligned} \tag{17}$$

The corresponding solution can be obtained by solving the hydrodynamic problem, using the newly found boundary conditions. Nevertheless, it can also be directly computed by using the matrix S^{-1}, which is assumed to be known

$$\begin{aligned} \hat{\alpha} = \alpha + \delta\alpha = \alpha + S^{-1}\boldsymbol{\varepsilon} = \alpha + (S^{-1}) \\ \times [(S^{-1})^* \, T^* M^p T(S^{-1}) + M^{q'} + C^* M^{w'} C]^{-1} \\ \times (S^{-1})^* \, T^* M^p (\xi^d - T\alpha) \end{aligned} \tag{18}$$

which is equivalent to

$$\hat{\alpha} = \alpha + \delta\alpha = \alpha + [T^* M^p T + S^*(M^{q'} + C^* M^{w'} C) S]^{-1} \times T^* M^p (\xi^d - T\alpha). \quad (19)$$

4.3. *The Link with the Generalised Least Square Method*

At this stage, the theoretical aspect of the assimilation problem has been entirely described. Nevertheless it makes sense to retrieve Eq. (19) by using the generalised least square formulation (cf. Tarantolla and Valette[22]), carried out by Jourdin [25]. Following Eq. (14), Eq. (15) and Eq. (16), the cost function J can be expressed in matrix notation by

$$J = (\mathbf{e} - \delta\xi)^* M^p (\mathbf{e} - \delta\xi) + \varepsilon^* M^{q'} \varepsilon + \varepsilon''^* M^{w'} \varepsilon''.$$

Combining the perturbation of the solution on the one hand and the perturbation of the boundary conditions, on the other hand, yields

$$\begin{aligned} J &= (\mathbf{e} - T\delta\alpha)^* M^p (\mathbf{e} - T\delta\alpha) \\ &\quad + \delta\alpha^* S^* (M^{q'} + C^* M^{w'} C)\, S\delta\alpha \\ &= (\mathbf{e} - T\delta\alpha)^* C_d^{-1} (\mathbf{e} - T\delta\alpha) + \delta\alpha^* C_p^{-1} \delta\alpha \\ C_d^{-1} &= M^p, \qquad C_p^{-1} = S^*(M^{q'} + C^* M^{w'} C) S. \end{aligned}$$

The matrix C_d^{-1} is analogous with the inverse matrix of the covariance matrix of an *a priori* error in the observations and C_p^{-1} is analogous with the inverse matrix of the covariance matrix of an *a priori* error in the boundary conditions. In the space of the data (the tidal observations), the solution is

$$\hat{e} = e + \delta e = e + C_p^{-1} T^* S_d^{-1} (\xi^d - T\alpha), \quad \text{where} \quad S_d = C_d + T C_p T^*.$$

In the space of the parameters (the tidal elevation), the solution is

$$\hat{\alpha} = \alpha + \delta\alpha = \alpha + S_p^{-1} T^* C_d^{-1} (\xi^d - T\alpha), \quad \text{where} \quad S_p = T^* C_d^{-1} T + C_p^{-1}$$

which is identical to Eq. (19). In particular, the link between these two formulations confirms *a posteriori* that the solution of the optimisation method in the discrete domain is the discretisation of the solution in the continuous domain, as Jourdin has shown that all operators in the least square formulation are compatible with the finite element discretisation.

4.4. *Practical Aspects*

In practical cases, it was decided to use the formulation of Eq. (18), which implies a partial knowledge of the inverse matrix of S, i.e., the columns of the inverse matrix corresponding to the open boundary nodes. In order to simplify the notations, the $N \times N_b$ restriction of the inverse matrix of S will be noted S^{-1}. The coefficients of S^{-1} are obtained simultaneously with the necessary reference solution. During resolution of the direct problem, the inverse matrix is never explicitly described, so the necessary coefficients are computed by using an impulsional response method, i.e. by solving the system: S^{-1}: $N \times N_b$ matrix $[s_{i,j}^{-1}]$ defined by

$$[S] \begin{bmatrix} s_{1,j}^{-1} \\ \cdots \\ s_{n,j}^{-1} \end{bmatrix} = [L][U] \begin{bmatrix} s_{1,j}^{-1} \\ \cdots \\ s_{n,j}^{-1} \end{bmatrix} = \begin{bmatrix} \delta_{1j} \\ \cdots \\ \delta_{nj} \end{bmatrix}.$$

When using a Gauss elimination solver, the additional cost to a single resolution is very low if the matrix factorisation coefficients of U and L are stored because the solving procedure is fully vectored. This step has to be performed for each node j of the open boundaries, irrespective of the set of observations. Finally, the least-square formulation yields

N_d: number of observations

N_b: number of open boundary nodes

N_n: number of nodes needed to interpolate the solution at the stations

$\tilde{S}^{-1}$: $N_n \times N_b$ restriction of S^{-1}

$\tilde{T}$: $N_d \times N_n$ restriction of T

$\tilde{M}^{q'}$, $\tilde{M}^{r'}$, $\tilde{C}$: $N_b \times N_b$ restriction of $M^{q'}$, $M^{r'}$, C

$$[(\tilde{S}^{-1})^* \tilde{T}^* M^p \tilde{T} (\tilde{S}^{-1}) + \tilde{M}^{q'} + \tilde{C}^* \tilde{M}^{r'} \tilde{C}] \tilde{\varepsilon} = (\tilde{S}^{-1})^* \tilde{T}^* M^p \tilde{\mathbf{e}}.$$

The choice of the weights and their effects on the new boundary conditions and solution are a crucial point of the method. Direct evaluation of the observation weights may be computed from *a priori* error levels estimated from some information available concerning the tide gauges. In the same way, the perturbation weights may be computed from a priori error levels estimated by local intercomparisons between the original cotidal solutions, which have been used to extract the open boundary conditions, and data. In spite of its rigorous appearance, this weight determination method remains essentially subjective. Moreover, the information needed to complete the error levels may not be available (undocumented data, data lacking in the vicinity of open domain limits). Because of the uncertainties of quantifying *a priori* the confidence that may be placed in the observations and boundary conditions and the necessity of controlling the impacts of the weights, it is necessary to explore different configurations by computing several approximate of boundary conditions using different weights and/or different observation sets. This is why the formula-

tion of Eq. (18) was chosen, it is applicable in the present instance because the input parameters are perturbed only on a restricted number of nodes, i.e., the open limit nodes. Once the NxN_b coefficients of S^{-1} are computed and stored, the numerical cost of a guess is negligible. A preliminary estimate of the corresponding effects on a new simulation can then be made with the assistance of the computed value of the future solution at the data points used:

$$\hat{\xi} = \xi + \tilde{T}\tilde{S}^{-1}\varepsilon, \qquad \hat{e} = \mathbf{e} - \tilde{T}\tilde{S}^{-1}\varepsilon.$$

Moreover, some null weighted pseudo-observations can be introduced into the observation set in order to have a "quick" look at the optimal solution in some particular parts of the domain. So the full system does not have to be solved each time as it has to be for an overall assimilation (which may take into account each node of the domain) and a prospective, semi-empirical methodology can easily be followed. In order to simplify the search for appropriate weights, it is useful to consider two separate aspects of the problem : the overall balance between the weights assigned to the solution misfits and those assigned to the boundary condition perturbation, on the one hand, and the modulation of the weights, normalised to unity, in each group, on the other hand. In fact, the reduction of RMS can be adjusted by modifying the overall balance,

$$J(\varepsilon) = \lambda \times \left(\sum_{\text{observations}} p_i^2 \, |e_i - \delta\xi_i|^2 \right) + (1-\lambda) \times \left(\int_{\Gamma_2} q^2 \, |\delta\alpha^0|^2 \, ds + \int_{\Gamma_2} w^2 \, |\delta\alpha^{0''}|^2 \, ds \right),$$

where $\sum_{\text{observations}} p_i^2 = 1$ and $\int_{\Gamma_2} q^2 \, ds + \int_{\Gamma_2} w^2 \, ds = 1$, and λ is the adjusting coefficient of the overall balance: $b^\lambda = \lambda/(1-\lambda)$ where $0 \leqslant \lambda \leqslant 1$.

It must be born in mind that the solution misfit is due not only to imperfect boundary conditions and that boundary condition optimisation should be carried out carefully. Certain particular processes are not taken into account in the present model, such as the interaction between barotropic and baroclinic tides. Despite a high resolution mesh, some local effects are not well modelled, such as the very short length diurnal topographic waves. Last but not least, data may contain survey and analysis errors of unsuspected magnitude. Certain discretisation errors can also occur when describing the geophysical domain, especially as a result of imperfect knowledge of the bottom topography. Thus it is necessary to define a limit which should not be overrun and to adjust the weight balance with that aim. Of course, the technique used here preserves the hydrodynamic nature of the "optimised" solution, in particular, mass conservation, but going beyond this limit will result in unrealistic and irrelevant new open boundary conditions.

Determining this limit is a difficult problem, as no exact criterion can be defined and empirical methods have to be used. It now appears necessary to seek a formalisation of this determination by selecting a set of criteria. One possible criterion is to examine the degree of efficiency of the optimisation procedure when the overall balance adjustment varies. When data are underweighted, the ratio between the reduction of the misfit between the observations and the solution, and the perturbation level are high. Conversely, when data are over-weighted, this ratio is very low. An illustration of this graph is shown on Fig. 9. The behaviour of the optimisation can thus be separated into three phases: quick decrease of the misfit, intermediate phase, slow decrease of the misfit. The limits of the method can probably be found in the intermediate phase and preliminary studies have shown that this phase is relatively sharp, so a first estimate of b^λ could be obtained from a graph of the optimisation procedure's efficiency. A similar criterion has been studied by McIntosh and Bennett [23]. They also propose an additional criterion which is that the a posteriori error levels have to be the same as the a priori error levels to consider the new solution as being acceptable. This criterion implies that one should be able to evaluate precisely the a priori error levels, which is rarely the case.

4.5. *Amendments to the Dominant wave case*

This optimisation technique is developed in a linear problem frame. In the case of the dominant wave simulation, the solving process is only *quasi*-linear. *A priori* knowledge of the dominant wave velocity field is theoretically necessary to estimate the bottom friction coefficients r, r', r'', r''' for any wave in the spectrum. Because of the lack of reliable overall ocean velocity fields, the dominant wave is resolved through an iterative process by initialising the wave's velocity with a uniform velocity field and then solving the elevation and deriving a new velocity field from Eq. (34) and Eq. (35) until the friction coefficients converge. So, although each step of the process is strictly linear, the overall procedure is nonlinear. It is possible to write at step i,

$$\alpha^i = M(\alpha^{i-1})\, F(\alpha^{i-1}) = M^i(\alpha^0)\, F^i(\alpha^0)$$

α^i: solution at step i

α^0: initial state of the solution, only defined on the open boundary.

The initial state is the virtual state corresponding to the initialisation velocity field and coinciding on the open boundaries with the boundary conditions (as do any of the successive solutions). At the convergence:

$$M(\alpha^0) = \lim_{i \to \infty} M^i(\alpha^0), \qquad F(\alpha^0) = \lim_{i \to \infty} F^i(\alpha^0).$$

Considering a second simulation which is identical to the first except that the initial state is modified by adding a perturbation to the open boundary conditions, the successive matrix and forcing vectors will also be perturbed, giving:

$$M(\alpha^0+\delta\alpha^0)=\lim_{i\to\infty} M^i(\alpha^0+\delta\alpha^0)=M(\alpha^0)+\delta M(\alpha^0,\delta\alpha^0)$$

$$F(\alpha^0+\delta\alpha^0)=\lim_{i\to\infty} F^i(\alpha^0+\delta\alpha^0)=F(\alpha^0)+\delta F(\alpha^0,\delta\alpha^0).$$

In order to simplify the notation, let

$$M(\alpha^0)=\mathcal{M}(0),\qquad M(\alpha^0+\delta\alpha^0)=\mathcal{M}(\delta\alpha^0),$$
$$\delta M(\alpha^0,\delta\alpha^0)=\delta\mathcal{M}(\delta\alpha^0)$$
$$F(\alpha^0)=\mathcal{F}(0),\qquad F(\alpha^0+\delta\alpha^0)=\mathcal{F}(\delta\alpha^0),$$
$$\delta F(\alpha^0,\delta\alpha^0)=\delta\mathcal{F}(\delta\alpha^0).$$

Subtracting the reference solution from the perturbed solution yields

$$\delta\alpha=\mathcal{M}(\delta\alpha^0)\,\mathcal{F}(\delta\alpha^0)-\mathcal{M}(0)\,\mathcal{F}(0)$$
$$=\mathcal{M}(0)\,\delta\mathcal{F}(\delta\alpha^0)+\delta\mathcal{M}(\delta\alpha^0)\,\mathcal{F}(0)+\delta\mathcal{M}(\delta\alpha^0)\,\delta\mathcal{F}(\delta\alpha^0).$$

The perturbation of the forcing term can be separated into two terms,

$$\delta\mathcal{F}(\delta\alpha_0)=\delta\alpha^0+\delta\mathcal{F}'(\delta\alpha^0),$$

where $\delta\alpha^0$ is the vector which coincides on the open limits with the perturbation of the boundary condition and is null inside the domain. $\delta\mathcal{F}'(\delta\alpha^0)$ is null on the open limits and coincides with the perturbation of the right side term of the variational equation (due to perturbation of the friction coefficients) inside the domain. Finally, ignoring the second-order term yields

$$\delta\alpha\approx \underbrace{\mathcal{M}\,\delta\alpha_0}_{\text{linear term}}+\underbrace{\delta\mathcal{M}(\delta\alpha_0)\,\mathcal{F}(0)+\mathcal{M}(0)\,\delta\mathcal{F}'(\delta\alpha_0)}_{\text{nonlinear terms}}$$

at the first order.

It is necessary here to assume that the nonlinear terms are negligible compared to the linear term. The optimisation method can thus be applicable to the dominant wave case. The nonlinear terms are due to the bottom friction coefficients and Table II indicates that they are quasi-insignificant outside the shallower area. Moreover, numerical experiments have shown that the elevation in deep ocean is smoothly dependent upon the velocity field, which is not the case in coastal regions. In order to ensure a favourable frame to the "linearity" assumption, three criteria should be applied. First, the reference simulation must already be of a high level of accuracy. In that case, the order of magnitude of the perturbation leading to the "optimal" solution is lower. Second, observations from high gradient areas must be removed from the optimisation data set. Third, the calculation of the new solution may no longer be computed by using the stored coefficients of S^{-1}, but by solving the linear system through a new iterative run. This verifies *a posteriori* that the nonlinear effects are slight in the vicinity of the data points. The validity of this assumption when these three criteria are respected has been verified *a posteriori* by successfully employing the boundary condition optimisation method to the simulation of the M_2 tide over realistic domains such as the Atlantic and Indian Oceans.

TABLE II

Characteristic Values in the Different Oceanic Areas

Parameter	Deep ocean, shelves	Coastal regions
ω	$1.405189\times10^{-4}\ s^{-1}$	$1.405189\times10^{-4}\ s^{-1}$
2Ω	$1.454441\times10^{-4}\ s^{-1}$	$1.454441\times10^{-4}\ s^{-1}$
C	2.50×10^{-3}	2.50×10^{-3}
u	10^{-3} to 10^{-1} m/s^{-1}	10^{-1} to 10^{0} m/s^{-1}
H	10^{4} to 10^{2} m	10^{2} to 10^{1} m
r, r'	10^{-12} to $10^{-7}\ s^{-1}$	10^{-7} to $10^{-4}\ s^{-1}$

Note. The magnitude of friction coefficient variation between deep ocean and very shallow regions is extremely high.

In conclusion, a method is proposed here to improve the tidal solutions of our hydrodynamic model by reducing the misfits with observations chosen inside the domain. Restrictions on this method are essentially that it can operate correctly only if boundary conditions are the dominant source of error. This method is of course less comprehensive than the full inverse problem methods which can operate directly inside the modelling domain. But it has several advantages. The first advantage is in its numerical cost (in terms of CPU memory size and time), which is much lower than for a complete inverse simulation. This lower computational cost means that it is possible to examine several guesses at boundary conditions, the effects of which on a new simulation can be quickly estimated. A similar empirical process may not be applicable when using an inverse problem method on a large oceanic basin. The second advantage is the conservation of the hydrodynamic properties of the optimised solutions. In particular, mass conservation is not perturbed as may be the case in an inverse method (see Bennett and McIntosh [24], and Jourdin [25]).

4. APPLICATION TO THE NORTH ATLANTIC BASIN

Oceanic tide M_2 was first modelled in the North Atlantic Basin, prior to the other oceanic basins. This gave the opportunity of testing the effect of the two above-mentioned optimal procedures on the level of accuracy of the model. This level of accuracy will also be compared to that of the CR [7] and NSWC [26] M_2 solutions. The modelling

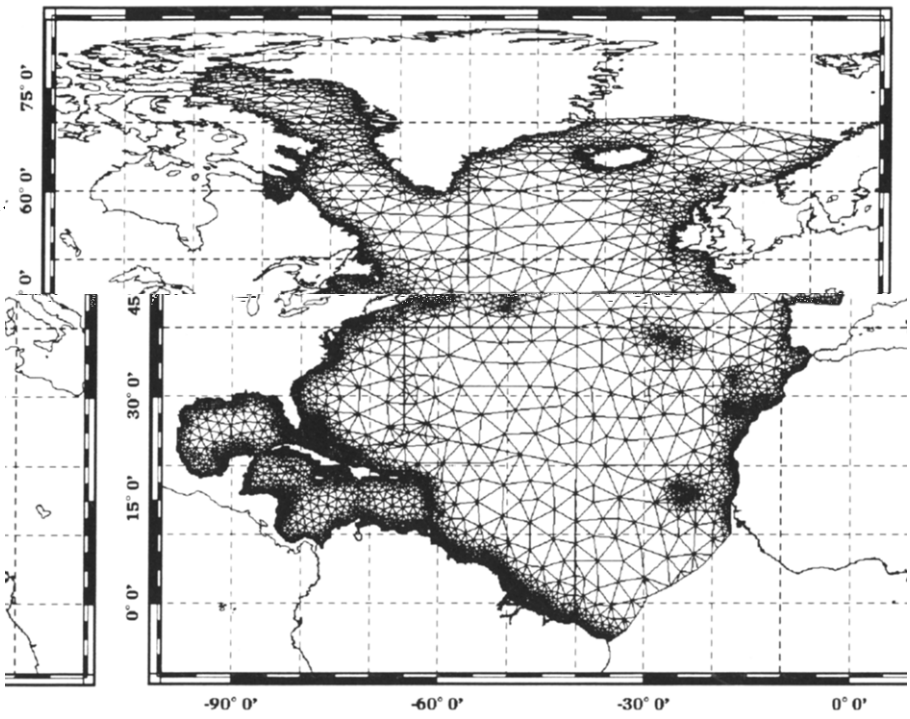

FIG. 2. Model Mesh. The mesh size, constrained by the bathymetry, varies from 30 km on the rigid boundaries to 400 km in the deep ocean. The equivalent spatial resolution in Lagrange-P2 approximation is respectively 15 km and 200 km. The high spatial resolution can be observed over the continental shelves.

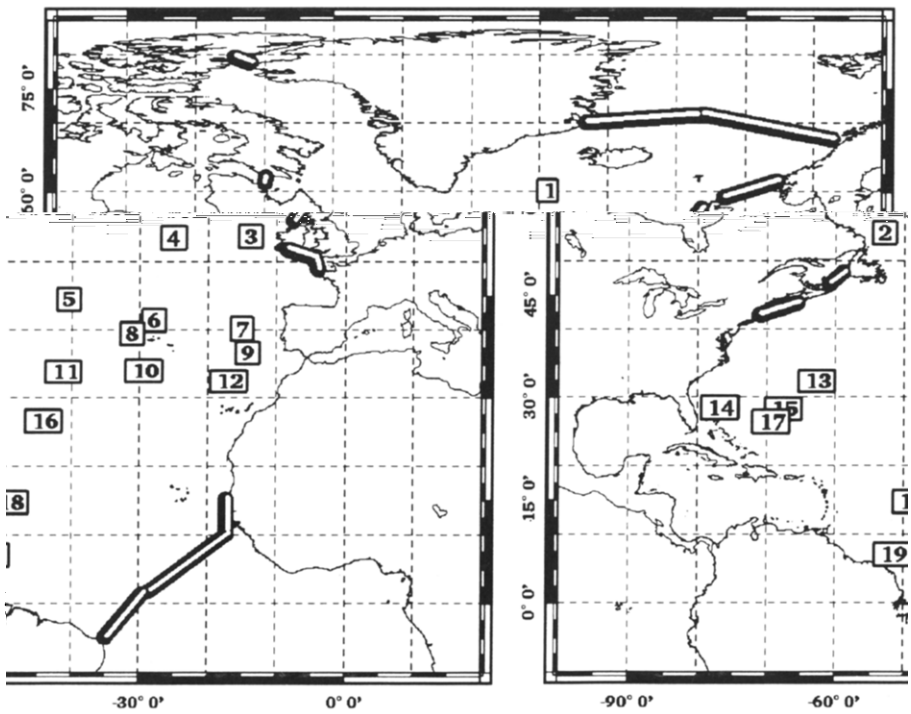

FIG. 3. Control stations set. It coincides on the domain with the set used by Cartwright and Ray [7] to estimate the accuracy level of their solution derived from the GEOSAT satellite records. All the stations are situated in the deep ocean. The open boundaries of the domain are represented by the thick black and white lines.

domain runs from approximately 0° South to 75° North and is represented in Fig. 2. The location of the main northern oceanic boundary was determined because of the existence of the regional model of Flather [20] and the need to avoid being close to the amphidromic points known to exist between Iceland and Scotland. The southern oceanic boundary follows a chain of observation sites, where data consistent with the oceanic tide are available. Along the continents, semi-closed bays and seas were excluded by setting open boundaries at their entrances, relying on *in situ* data or high-precision local models when available, i.e., the North Sea, the English Channel [27], the Gulf of Main [28], and the Gulf of St. Lawrence. Most of the *in situ* data were drawn from the IAPSO data bank [29, 30, 31] and the IHO [32] data bank. At the contrary, the domain includes the Caribbean Sea, the Gulf of Mexico, and the Baffin Sea. Islands are taken into account when their typical dimensions are greater than 30 km. The domain contains 11642 elements and 25716 nodes in the Lagrange-P2 approximation and there are 333 open boundary nodes (see Fig. 3). The loading and self-attraction effects were taken from the overall charts of Francis and Mazzega [33].

The number of deep ocean tidal gauge sites in the North Atlantic is very important. This set can also be extended with observations obtained from shelf stations. The spatial distribution is not really homogenous but almost. In order to be consistent with the comparisons made by Cartwright and Ray between the CR model and observations, the same set of accuracy control observations has been kept (see Fig. 3 and Table III).

TABLE III

Location and Name of the Control Set Stations, in Eastward Longitude and Northward Latitude

N°	Stations	Longitude	Latitude
1	IAPSO.1.1.30	−28°46′	60°12′
2	P694	−52°54′	54°0′
3	IAPSO.1.1.35	−13°51′	53°35′
4	IAPSO.1.1.33	−25°6′	53°31′
5	IAPSO.1.2.36	−40°30′	44°28′
6	IAPSO.1.1.40	−27°57′	41°25′
7	IAPSO.1.1.74	−15°3′	40°17′
8	Flores Island	−31°7′	39°28′
9	IAPSO.1.1.42	−14°15′	36°40′
10	IAPSO.1.1.72	−29°23′	33°58′
11	IAPSO.1.2.38	−41°10′	33°55′
12	Funchal (Madeira)	−16°55′	32°28′
13	St. George (Bermuda)	−62°42′	32°22′
14	IAPSO.1.2.15	−76°48′	28°27′
15	IAPSO.1.2.5	−67°31′	28°13′
16	IAPSO.1.2.39	−43°58′	26°34′
17	IAPSO.1.2.9	−69°19′	26°27′
18	IAPSO.1.3.13	−48°49′	14°41′
19	IAPSO.1.3.15	−51°32′	7°0′

Note. Most of the stations come from the IAPSO data bank.

5.1. *The Reference Solution*

In order to enable comparisons to be made between the two optimisation procedures, a reference solution has to be defined. As the optimised bathymetry in theory ensures better matrix coefficients, it has to be used in the open boundary condition optimisation. Otherwise, the relation between the boundary conditions and inner values of the solution would be affected and might lead to inconsistent perturbations of the optimal boundary conditions. Thus the reference solution, noted CEF1, was computed with an already optimised bathymetry and is shown on Figs. 4 and 5. The time-dependent discrepancy between the observations and the solution is defined by $d_i(t) = [a\cos(\omega t - G)]_i^{\text{data}} - [a\cos(\omega t - G)]_i^{\text{model}} = \Re(\alpha_i^{\text{data}} \exp(j\omega t)) - \Re(\alpha_i^{\text{model}}(\lambda_i, \varphi_i) \exp(j\omega t)) = \Re(\delta\alpha_i \exp(j\omega t))$, where $\delta\alpha_i$ is the complex difference: $\delta\alpha_i = \alpha_i^{\text{data}} - \alpha^{\text{model}}(\lambda_i, \varphi_i) = d_i \exp(j\theta_i)$; d_i represents the greatest discrepancy which can be observed [illegible]. The RMS of the maximum misfits between the

where | | denotes the complex modulus. The RMS of the time averaged misfits with the control observation constants, noted RMS*, is defined by

$$\text{RMS}^* = \sqrt{(1/N)\sum_N [(1/T)\int_0^T [d_i(t)]^2\, dt]}$$
$$= \sqrt{(1/N)\sum_N [(1/T)\int_0^T (d_i\cos(\omega t + \theta_i))^2\, dt]}$$
$$= \frac{\sqrt{2}}{2}\,\text{RMS}.$$

(As both definitions give analogous estimates, either the first or the second can be used to evaluate the performances of the model. In the following, the first one will be retained as the second one is not explicitly mentioned.) The level of accuracy in terms of the RMS of this solution is of the same order as the NSWC and CR models as shown in Table V.

5.2. *Bathymetry Optimisation*

The smoothed and optimally designed bathymetries were not represented here because they are too close to enable a

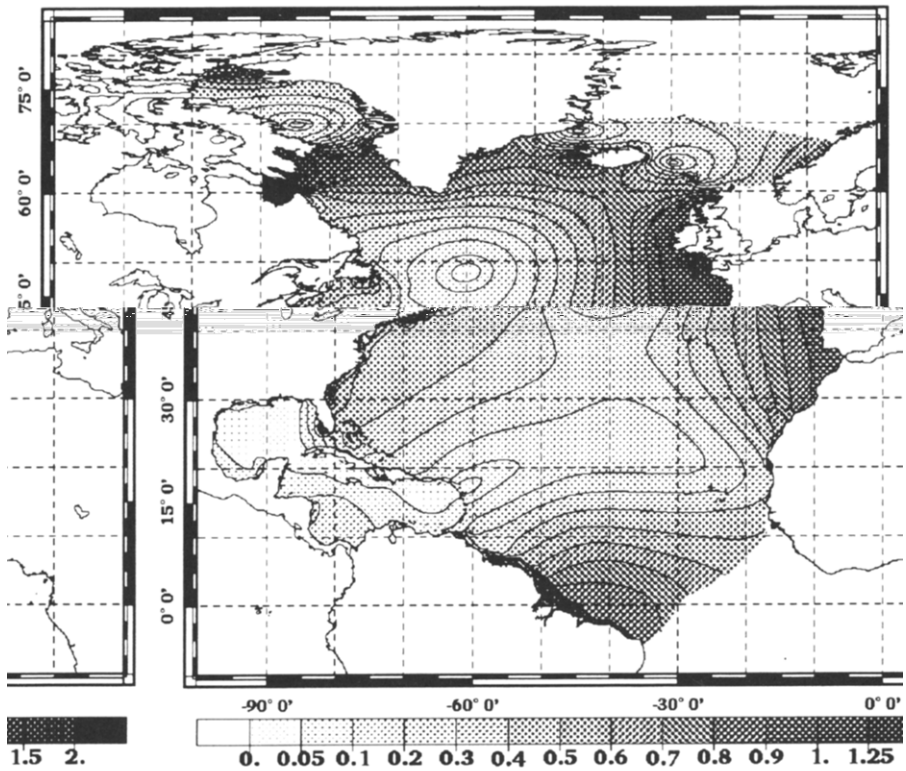

FIG. 4. Chart of the M_2 amplitude in metres of the reference solution CEF1. The magnitude is at its minimum on the amphidromic points and ncreases on continental shelves.

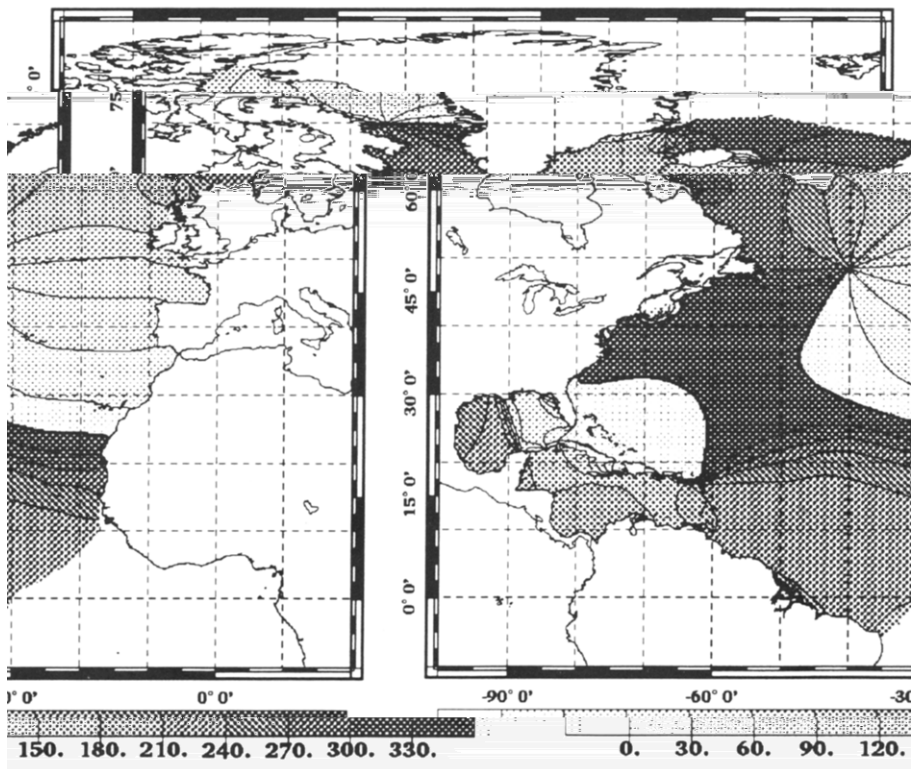

FIG. 5. Chart of the M_2 phase lag in degrees of the reference solution CEF1. Phases turn around the amphidromic points.

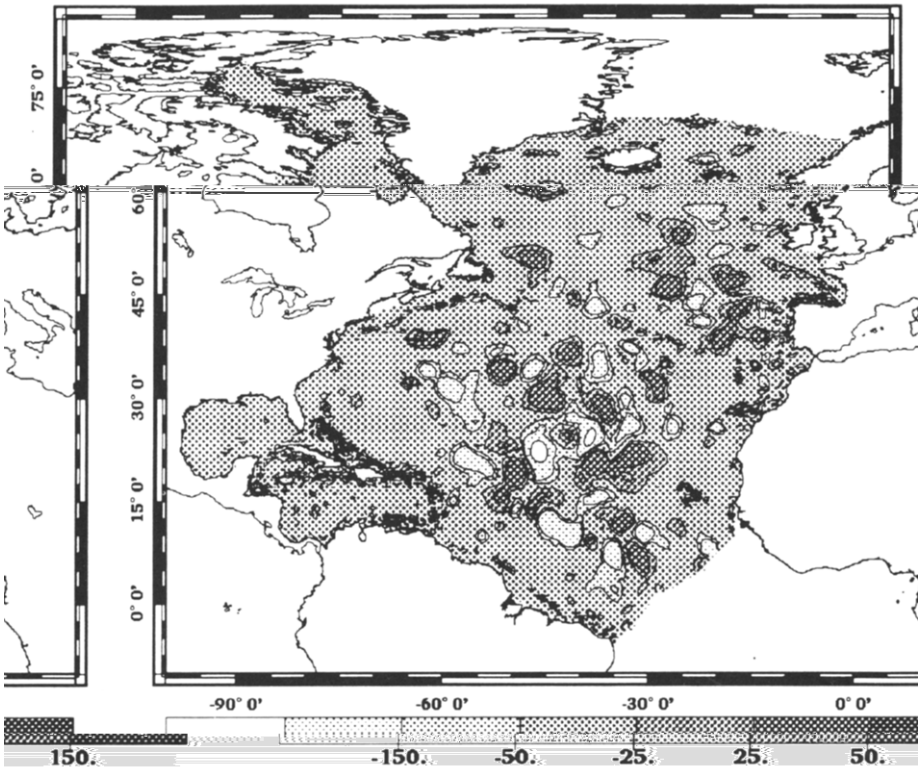

FIG. 6. Chart in metres of the difference between the classically smoothed and optimised model bathymetries. The difference is mainly in the range between -25 m and $+25$ m. The difference is most significant on the continental edges and over the Atlantic Ridge.

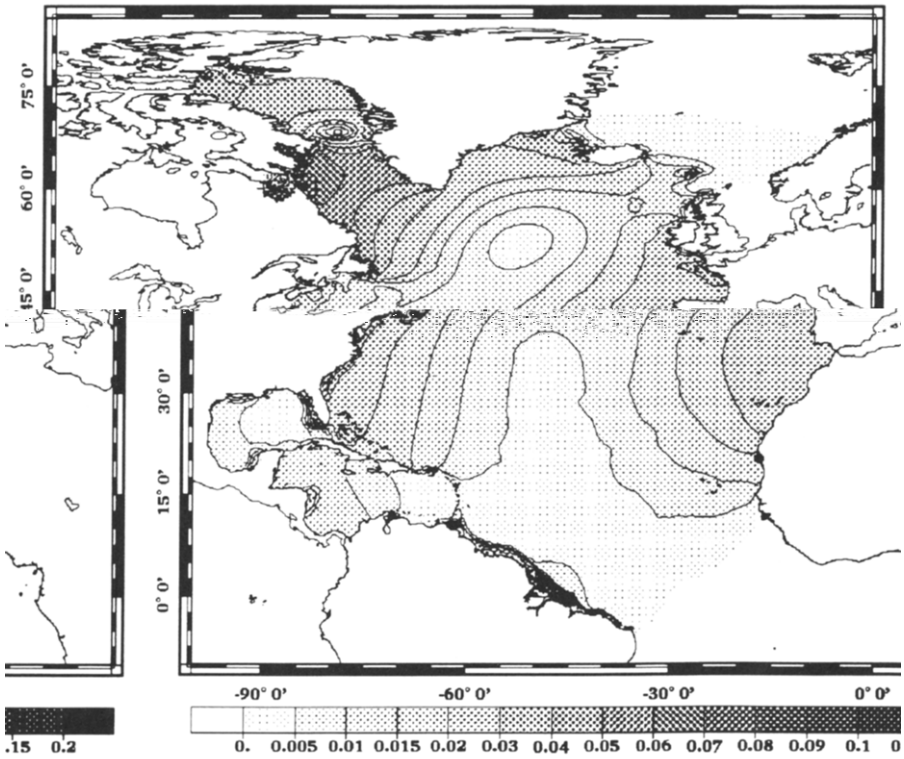

FIG. 7. Amplitude in metres of the complex difference between the M_2 solution computed with an optimised bathymetry (CEF1) and a classically smoothed bathymetry (CEF2). The difference is maximum in the Labrador Basin (4 to 7 cm).

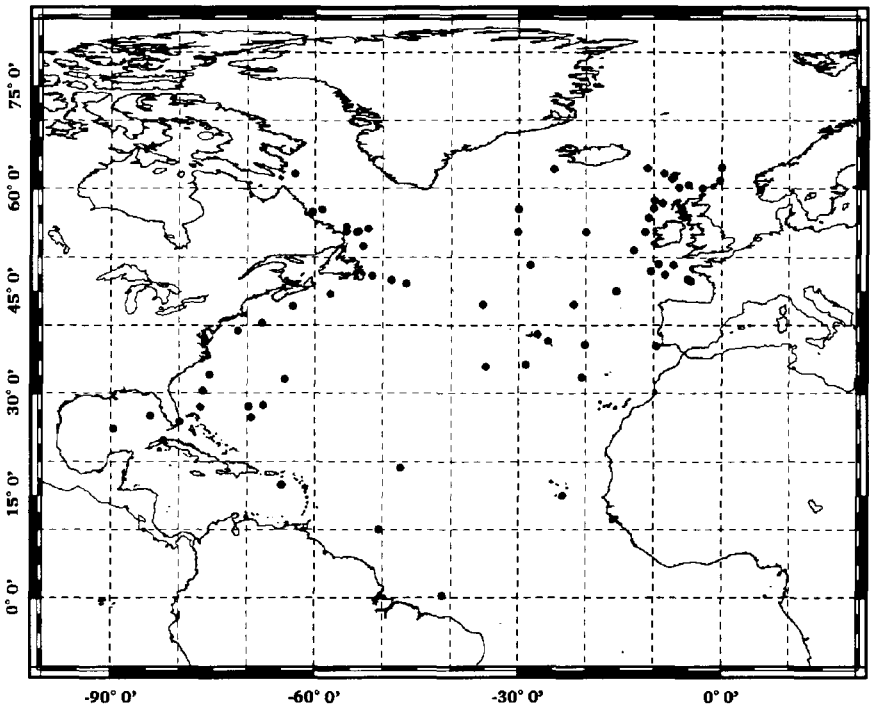

FIG. 8. Location of the stations used in the boundary condition optimisation procedure (black circles). Only shelf and pelagic stations have been included in the optimisation set. The optimisation and control set have no common element.

level (0.5 to 3 cm) appears in the centre of the basin. It reaches about 6 cm on the continental coasts and rises to more than 10 cm in the Labrador Basin. The mean absolute difference over the domain is 3.3 cm and the corresponding RMS is 3 cm.

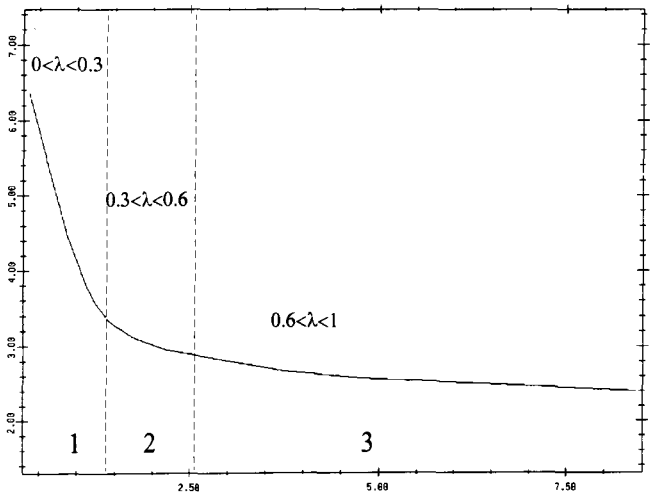

FIG. 9. Magnitude in centimeters of the residual (after optimisation) RMS between the observations and the solution (vertical axis) versus magnitude of the perturbations of the boundary conditions (horizontal axis): 1 is a good working area, 2 is a transition area, 3 is a bad working area. The global balance has been chosen to fit the limit between the areas 1 and 2; λ is the adjusting coefficient in the cost function $J(\varepsilon) = \lambda \times (\sum_{\text{observations}} P_i^2 \, |e_i - \delta\zeta_i|^2) + (1-\lambda) \times (\int_{\Gamma_2} q^2 \, |\delta\alpha^0|^2 \, ds + \int_{\Gamma_2} w^2 \, |\delta\alpha^{0''}|^2 \, ds)$.

The inter-comparisons between CEF1, CEF3 and observations of the control set are presented in Table IV. Differences which are greater than the RMS of the amplitude (3.5 cm) and phase lag (5.3°) of CEF1 have been labelled with a star. The improvement in accuracy is obvious when comparing the number of labelled values in the CEF1 and CEF3 columns. The CEF3 amplitude misfit is less than 3 cm at each station and the solution shows a phase lag misfit which is over 5° at only two stations. The amplitude RMS decreases to 1.3 cm and the phase lag RMS decreases to 3.7°. The last three columns illustrate the level of accuracy of the CEF solutions in terms of maximum error, which takes into account both amplitude and phase misfits. Most of the stations show a gain in accuracy (represented by the negative values). The only significant increase in the misfit occurs for station 10. As the optimisation method is based on least square procedures, it levels the misfits by decreasing the greatest and possibly increasing the lowest ones when they are partially inconsistent with the other data. The maximum misfit (9.9 cm) is observed at station 9 and is essentially due to a phase lag misfit ($-6.6°$) combined with a large amplitude (~ 86 cm). It should be noted that the CR model indicates a similar misfit (-1.6 cm and $-8.2°$) at this station. Comparing this station to other stations situated in the same area showed that station 9 may present a problem on the M_2 tidal constants and should be removed from the control set. However, in order to maintain the same control set as Cartwright and Ray, it was retained for this paper.

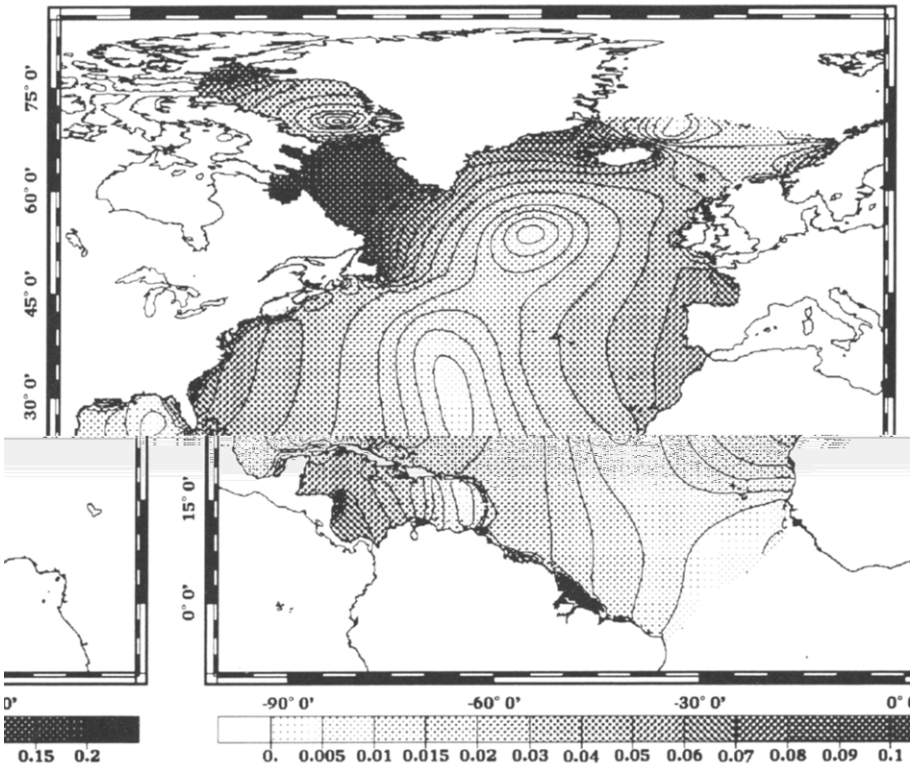

FIG. 10. Amplitude in metres of the complex difference between the M_2 solution computed with the initial boundary conditions (CEF1) and with the optimised boundary conditions (CEF3). The difference is at its maximum in the Labrador Basin (10 to 20 cm).

Subsequently, it should be removed for any station intercomparison set. However, the overall level of accuracy, in terms of the above RMS, which indicates the RMS of the maximum misfits, is 3.2 cm. The timeaverage of the complex error leads to an RMS* of 2.2 cm and should be compared

domain. The second method consists in assimilating tidal data inside the modelling domain by seeking the optimum boundary conditions which will minimise misfits between the observations and the solution. This method is based on

TABLE IV

Intercomparisons with the *in situ* Data of the Control Set Stations

	Observations		CEF1				CEF3				CEF1	CEF3	
N°	*a*	*G*	*a*	*G*	*Δa*	*ΔG*	*a*	*G*	*Δa*	*ΔG*	*d*	*d*	*Δd*
1	69.9	183.0	67.1	184.2	−2.5	1.2	70.0	185.5	0.4	2.5	2.9	3.1	+0.2
2	40.2	297.0	36.3	282.8	*−3.9	*−14.2	41.5	292.8	−1.3	−4.2	10.2	3.3	−6.9
3	98.3	142.0	91.2	144.5	*−7.1	2.5	95.3	144.0	−3.0	2.0	8.2	4.5	−3.7
4	52.6	145.0	49.7	148.3	−2.9	3.3	51.2	147.9	−1.4	2.9	4.1	3.0	−1.1
5	14.7	31.0	13.0	22.0	−1.7	*−9.0	14.5	26.0	−0.2	−5.0	2.8	1.3	−1.5
6	46.7	73.0	43.0	71.5	*−3.7	−1.5	45.9	71.4	−0.8	−1.6	3.9	1.5	−2.4
7	88.0	74.0	80.7	73.9	*−7.3	−0.1	85.3	74.2	−2.7	0.2	7.3	2.7	−4.6
8	38.5	59.0	35.5	54.9	−3.0	−4.1	37.8	55.5	−0.7	−3.5	4.0	2.4	−1.6
9	85.6	68.0	81.6	60.8	*−4.0	*−7.2	86.4	61.4	0.8	*−6.6	11.2	9.9	−1.3
10	36.7	43.0	36.3	42.6	−0.4	−0.4	38.7	43.9	2.0	0.9	0.5	2.1	+1.6
11	25.7	10.0	26.8	11.3	1.1	1.3	27.0	12.3	1.3	2.3	1.3	1.7	+0.4
12	72.1	46.0	68.8	44.9	−3.3	−1.1	72.9	46.0	0.8	0.0	3.6	0.8	−2.8
13	35.7	358.0	37.8	359.0	2.1	1.0	35.2	355.3	−0.5	−2.7	2.2	1.7	−0.5
14	40.8	2.0	44.4	6.2	*3.6	4.2	40.7	0.7	0.1	−1.3	4.8	0.9	−3.9
15	34.0	359.0	36.0	4.0	2.0	5.0	33.1	359.0	−0.9	0.0	3.6	0.9	−2.7
16	15.0	329.0	15.9	341.3	0.9	*12.3	16.0	339.9	1.0	*10.9	3.4	3.1	−0.3
17	31.7	0.0	34.9	6.6	3.2	*6.6	32.0	1.3	0.3	1.3	5.0	0.8	−4.2
18	32.9	233.0	31.4	229.0	−1.5	−4.0	32.7	231.1	−0.2	−1.9	2.7	1.1	−1.6
19	57.3	222.0	54.9	218.0	−2.4	−4.0	55.7	219.9	−1.6	−2.1	4.6	2.6	−2.0
RMS					3.5	5.3			1.3	3.7			

Note. Tidal amplitude (a) in centimeters, phase lag (G) in degrees, related to Greenwich, amplitude of the complex difference (d) in centimeters. The differences marked with an asterisk those are whose absolute value is greater than the corresponding RMS computer for the CEF1 solutions. A negative value of *Δd* means an improvement with respect to the reference solution CEF1.

for comparisons. Thus, although the boundary condition optimisation method is not as sophisticated as some existing assimilation methods, it considerably improves the accuracy of the tidal solution with a much lower numerical cost and is easier to use than a full assimilation method. Coming back to the accuracy required in tidal applications, the use of bathymetry and boundary condition optimisation methods appears to be an essential step in meeting these objectives in relation with the present hydrodynamic tidal modelling approach.

TABLE V

RMS and RMS* of the Misfits between Observations and Solutions, in Centimetres, Computed with the Control Station Set

	NSWC	CR	CEF1	CEF2	CEF3
RMS	6.4	4.4	5.3	5.8	3.2
RMS*	4.5	3.1	3.7	4.1	2.3

Note. The accuracy of the CEF1 and CEF2 solutions is in the range between those of NSWC and CR. The accuracy of CEF3 is the best of all. RMS is related to the maximum in time misfits; RMS* is related to the averaged in time misfits.

APPENDIX I: MODEL FORMULATION AND BOUNDARY CONDITIONS

Below is a fully detailed description of the hydrodynamic model developed by Le Provost and Vincent [11].

1.1 *The Basic Equations*

The continuity equation is

$$\frac{\partial h}{\partial t} + \nabla \cdot (h\mathbf{u}) = 0. \tag{20}$$

The momentum equation, in its nonconservative form is

$$\frac{\partial \mathbf{u}}{\partial t} + \vec{\nabla}(u)\mathbf{u} + g\nabla\alpha + \frac{C_f}{h}\|\mathbf{u}\|\mathbf{u} + 2\boldsymbol{\Omega} \wedge \mathbf{u} = \nabla\Pi \tag{21}$$

with

α, sea surface denivellation

h, instantaneous water depth: $h = H + \alpha$

$\mathbf{u}$, barotropic velocity

Π, tidal potential

$\mathbf{\Omega}$, Earth's rotation: $f = 2\Omega \sin \varphi$

C_f, dimensionless friction coefficient (typically 2.5×10^{-3}).

Following Hendershott [34]], tidal potential takes the form

$$\Pi(\lambda, \varphi) = g\left[(1 + k_2 - h_2)\frac{\Pi_2(\lambda, \varphi)}{g} + \iint \alpha(\lambda', \varphi')\, G(\lambda, \varphi, \lambda', \varphi') \cos \varphi'\, d\lambda'\, d\varphi'\right]$$

with

(a, λ, φ): geocentric coordinates

$\Pi_2(\lambda, \varphi)$: astronomical potential

h_n, k_n: Love numbers

$G(\lambda, \varphi, \lambda', \varphi')$: Green's loading function,

where λ is the eastward longitude east of Greenwich and φ is the latitude north. Actually, Π_2 is the first term of the expansion (in Legendre polynomials) of the complete astronomical potential.

1.2. *The Model Equations*

The formulation developed by Le Provost *et al.* [3] is summarised here. Assuming the spectral expansion in time of the tidal unknowns, derived from the discrete spectrum of the tidal potential:

t: Greenwich Mean Time (universal time)

V_{0k}: initial phase of the equilibrium constituent k at Greenwich

ω_k: frequency of constituent k

$$\Pi_2 = \sum_k \Pi_{2k} \exp(js\lambda) \exp(j[\omega t + V_{0k}]) + \text{c.c}$$

where s depends on the species of the constituent k ($s = 1$ for diurnal tides, $s = 2$ for semi-diurnal tides). Elevation and velocity are expanded in a similar way:

$$\alpha_k(\lambda, \varphi) = a_k \exp(-jG_k), \qquad \mu_k(\lambda, \varphi) = u_k \exp(j\psi_k),$$

$$v_k(\lambda, \varphi) = v_k \exp(j\chi_k)$$

$$h(\lambda, \varphi, t) = H(\lambda, \varphi) + \sum_k \alpha_k(\lambda, \varphi) \exp(j[\omega_k t + V_{0k}]) + \text{c.c.}$$

$$u_\lambda(\lambda, \varphi, t) = u_\lambda^0(\lambda, \varphi) + \sum_k \mu_k(\lambda, \varphi) \exp(j[\omega_k t + V_{0k}]) + \text{c.c.}$$

$$u_\varphi(\lambda, \varphi, t) = u_\varphi^0(\lambda, \varphi) + \sum_k v_k(\lambda, \varphi) \exp(j[\omega_k t + V_{0k}]) + \text{c.c.}$$

The existence of a dominant wave (α_1, μ_1, v_1) in terms of velocity (such as the mean lunar tide M_2 in the North Atlantic) allows the bottom friction term to be linearised (Kabbaj and Le Provost [35]]) for any waves in the tidal spectrum:

$$\left[\frac{C_f}{H}\|\mathbf{u}\|\,\mathbf{u}\right]_k = \begin{bmatrix} r\mu_k + r'v_k \\ r''\mu_k + r'''v_k \end{bmatrix},$$

where r, r', r'', r''' depend only on the dominant wave velocity field (μ_1, v_1). Bottom friction terms related to the dominant wave are

$$r = r''' = \frac{C_f}{H}R, \qquad r' = -r'' = j\frac{C_f}{H}R'. \tag{22}$$

The terms R and R' are computed from the dominant wave velocity field:

$$R = \frac{1}{\sqrt{2}}\sqrt{\mu_1^2 + v_1^2}\left[G_{00} + \frac{G_{02}}{2J_1}\right] \tag{23}$$

$$R' = \varepsilon\frac{1}{\sqrt{2}}\sqrt{\mu_1^2 + v_1^2}\,\frac{G_{02}}{2J_1}(1 - J_1^2)^{1/2}. \tag{24}$$

Bottom friction terms related to the other waves are

$$r = \frac{C_f}{H}(R + R'), \qquad r' = r'' = \frac{C_f}{H}R'', \qquad r''' = \frac{C_f}{H}(R - R'). \tag{25}$$

The terms R, R' and R'' are computed from the dominant wave velocity field:

$$R = \frac{3}{2\sqrt{2}}\sqrt{\mu_1^2 + v_1^2}\,G_{00}, \tag{26}$$

$$R' = \frac{3}{2\sqrt{2}}\sqrt{\mu_1^2 + v_1^2}\,\frac{G_{02}}{2J_1}\,\frac{\mu_1^2 - v_1^2}{\mu_1^2 + v_1^2}, \tag{27}$$

$$R'' = \frac{3}{2\sqrt{2}}\sqrt{\mu_1^2 + v_1^2}\,\frac{G_{02}}{2J_1}\,\frac{\mu_1 v_1}{\mu_1^2 + v_1^2}\cos(\chi_1 - \psi_1), \tag{28}$$

where

$$J_1^2 = 1 - 4\frac{\mu_1^2 v_1^2}{(\mu_1^2 + v_1^2)}\sin^2(\psi_1 - \chi_1),$$

$$J = \sqrt{2J_1/(1 + J_1)}$$

$$\varepsilon = +1 \quad \text{if} \quad 0 < \psi_1 - \chi_1 < \pi,$$

$$\varepsilon = -1 \quad \text{if} \quad \pi < \psi_1 - \chi_1 < 2\pi$$

$$G_{00} = \frac{2^{3/2}}{\pi}(2 - J^2)^{-1/2}\,E(J)$$

$$G_{02} = \frac{2^{5/2}}{\pi}(2 - J^2)^{-1/2}\left\{E(J) + \frac{2(1 - J^2)}{J^2}[E(J) + F(J)]\right\};$$

E and F are the second- and first-order elliptic integrals.

For astronomical waves (i.e., waves which are generated directly by astronomical forcing), the spectral quasi-linearised system is

$$j\omega_k \alpha_k + \frac{1}{\quad}\left[\frac{\partial H\mu_k}{\quad} + \frac{\partial Hv_k \cos\varphi}{\quad}\right] = F_k^{\alpha} \qquad (29)$$

[redacted]

$$(j\omega_k + r)\,\mu_k + (r' - f)\,v_k + \frac{g}{a\cos\varphi}\frac{\partial \alpha_k}{\partial \lambda} = F_k^{\mu} \qquad (30)$$

$$(r'' + f)\,\mu_k + (j\omega_k + r''')\,v_k + \frac{g}{a}\frac{\partial \alpha_k}{\partial \varphi} = F_k^{v} \qquad (31)$$

Equation (32) is a second order elliptic equation where the elevation remains the only unknown.

1.3. *The Variational Formulation*

The tidal elevation corresponding to a wave of the spec[redacted]

under its variational formulation and application of Green's theorem yields:

Considering Ω the modelling domain, the Sobolev space H^1_{Ω} of the complex-valued functions and first derivatives square integrable on the domain Ω and introducing a class

friction coefficients; and second, solution of the other astronomical waves. The second problem is purely linear, whereas the first one is nonlinear through the iterative process.

APPENDIX II: FINITE ELEMENT DISCRETISATION

This appendix describes how the finite element technique is applied to the discretisation of the continuity equation. The basic element is the triangle, which contains three nodes in the Lagrange-P1 approximation, and six nodes in the Lagrange-P2 approximation. The interpolation polynomials P_i are defined on a reference rectangular triangle denoted R. Interpolation of a function f, known at the nodes of an element, is performed by transferring the computation into the reference triangle, using an affine transform, illustrated on Fig. 1:

T_l the affine transform: $\Omega_l \rightarrow$ Reference rectangular triangle

$$(\lambda, \varphi) \mapsto (x, y).$$

The index arrays are defined as follows:

$\eta(i, l)$: number of the node of Ω_l corresponding by the T_l transform to the ith node in R

$\iota(n, l)$: number of the node of R which is the image of the node n, belonging to Ω_l, by the T_l transform.

So the interpolated function f is defined over the element by

$$f(\lambda, \varphi)|_{\Omega_l} = \sum_{n \in \Omega_l} f_n P_{\iota(l,n)}(x, y). \tag{36}$$

The continuity equation (33) is discretised by seeking the solution α in the vectorial space V of the complex-valued polynomials of degree equal to or lower than the degree of the selected Lagrange approximation. Let N be the total number of nodes in the domain. A natural base B of V is the set of interpolation polynomials:

$$B = \{\beta_n, n \in [1, ..., N], \text{ where } \quad \beta_n|_{\Omega_l} \equiv 0 \quad \forall n \notin \Omega_l \quad \beta_n|_{\Omega_l} \equiv P_{\iota(l,n)} \quad \forall n \in \Omega_l. \tag{37}$$

The discrete solution can be written

$$\alpha(\lambda, \varphi) = \sum_{n=1}^{N} \alpha_n \beta_n(\lambda, \varphi). \tag{38}$$

The discretised formulation of Eq. (33) can be written

$$\tilde{W}_{\alpha^0}(\Gamma) = \{\alpha \in V / \alpha_\Gamma = \alpha^0\}.$$

Find a function α of $\tilde{W}_{\alpha^0}(\Gamma_2)$ such that

$$L(\alpha, \beta) = F(\beta), \qquad \forall \beta \in \tilde{W}_0(\Gamma_2). \tag{39}$$

A necessary and sufficient condition is that Eq. (39) must be verified by each element of a base of the vectorial space $\tilde{W}_0(\Gamma_2)$. A simple base of $\tilde{W}_0(\Gamma_2)$ is the subset of B related to the inner nodes of the domain (i.e., each node of the domain except those belonging to the open limits). In order to simplify the following developments, the two sets can be defined as

$$\Lambda_n = \{\text{elements } \Omega_l / \text{node } n \in \Omega_l\},$$
$$V_n = \{\text{nodes } m / \Lambda_n \cap \Lambda_m \neq \varnothing\}.$$

The nth equation of the hydrodynamic system is obtained by applying Eq. (39) to the nth base element. A particular term of $L(\alpha, \beta)$ is developed by

$$I_{A,n} = \iint_{\Omega} A(\lambda, \varphi) \frac{\partial \alpha}{\partial \varphi} \frac{\partial \bar{\beta}}{\partial \varphi} \cos \varphi \, d\lambda \, d\varphi = \sum_{\Omega} I^l_{A,n}, \tag{40}$$

where $I^l_{A,n}$ is the contribution of the element l to the discrete equation written for the nth basic polynomial. Substitution of Eq. (37) in Eq. (40) gives

$$I^l_{A,n} = \iint_{\Omega_l} A(\lambda, \varphi) \cos \varphi \frac{\partial}{\partial \varphi} \left(\sum_{m=1}^{N} \alpha_m \beta_m(\lambda, \varphi) \right) \frac{\partial \beta_n}{\partial \varphi} d\lambda \, d\varphi.$$

Because of the properties of the interpolation functions, $I^l_{A,n}$ is equal to zero for each element that does not contain the node n. So the integral can be simplified by

$$I_{A,n} = \sum_{\Omega_l \in \Lambda_n} I^l_{A,n} = \sum_{\Omega_l \in \Lambda_n} \left[\sum_{m \in \Omega_l} J^l_{A,m,n} \alpha_m \right], \qquad \text{where}$$
$$J^l_{A,m,n} = \iint_{\Omega_l} A(\lambda, \varphi) \cos \varphi \frac{\partial P_{\iota(m,l)}}{\partial \varphi} \frac{\partial P_{\iota(n,l)}}{\partial \varphi} d\lambda \, d\varphi. \tag{41}$$

$J^l_{A,m,n}$ is the contribution of the node m m to the discrete equation written for the nth basic polynomial. Reorganising Eq. (41) by grouping the common terms related to the node n and its neighbour m yields

$$I_{A,n} = \sum_{m \in V_n} a_{n,m} \alpha_m, \qquad \text{where} \quad a_{n,m} = \sum_{\Omega_l \in (\Lambda_n \cap \Lambda_m)} = \sum_{\Omega_l \in (\Lambda_n \cap \Lambda_m)} \left[\iint_{\Omega_l} A(\lambda, \varphi) \cos \varphi \frac{\partial P_{\iota(m,l)}}{\partial \varphi} \frac{\partial P_{\iota(n,l)}}{\partial \varphi} d\lambda \, d\varphi \right]. \tag{42}$$

Following a similar development for each term of the continuity equation, the following coefficients can be defined:

$$t_{n,m} = \sum_{\Omega_l \in (\Lambda_n \cap \Lambda_m)} \left[\iint_{\Omega_l} j\omega \cos\varphi P_{i(m,l)} P_{i(n,l)}\, d\lambda\, d\varphi \right],$$

$$b_{n,m} = \sum_{\Omega_l \in (\Lambda_n \cap \Lambda_m)} \left[\iint_{\Omega_l} \frac{B(\lambda,\varphi)}{\cos\varphi} \frac{\partial P_{i(m,l)}}{\partial\lambda} \frac{\partial P_{i(n,l)}}{\partial\lambda}\, d\lambda\, d\varphi \right],$$

$$c_{n,m} = \sum_{\Omega_l \in (\Lambda_n \cap \Lambda_m)} \left[\iint_{\Omega_l} C(\lambda,\varphi) \frac{\partial P_{i(m,l)}}{\partial\lambda} \frac{\partial P_{i(n,l)}}{\partial\varphi}\, d\lambda\, d\varphi \right],$$

$$d_{n,m} = \sum_{\Omega_l \in (\Lambda_n \cap \Lambda_m)} \left[\iint_{\Omega_l} D(\lambda,\varphi) \frac{\partial P_{i(m,l)}}{\partial\varphi} \frac{\partial P_{i(n,l)}}{\partial\lambda}\, d\lambda\, d\varphi \right],$$

$$e_n = \sum_{\Omega_l \in \Lambda_n} \left[\iint_{\Omega_l} [BF_\mu - DF_\nu](\lambda,\varphi) \frac{\partial P_{i(n,l)}}{\partial\lambda}\, d\lambda\, d\varphi \right],$$

$$g_n = \sum_{\Omega_l \in \Lambda_n} \left[\iint_{\Omega_l} [AF_\nu - CF_\mu](\lambda,\varphi) \cos\varphi \frac{\partial P_{i(n,l)}}{\partial\varphi}\, d\lambda\, d\varphi \right].$$

Considering the general linear matrix S of the discrete problem, it is possible to write

$$S[\alpha] = F,$$

where

$$S = [s_{n,m}] = [-t_{n,m} + a_{n,m} + b_{n,m} - c_{n,m} - d_{n,m}]$$

and

$$F = [f_n] = \left[\frac{a}{g}(e_n + g_n)\right].$$

Nevertheless, the coefficients A, B, C, D are not discretised by a finite element procedure, so the integrals must be computed numerically. Numerical integration is performed by a classic Hammer method, which integrates exactly on a triangle the polynomials $x^i y^i$ when $i+j$ is equal to or smaller than a "total" degree m; m is dependent on the amount NPG of Gauss points that are used (cf. Dhat and Touzot [36]):

(x_k, y_k): coordinates in the reference triangle of the kth Gauss point in R

p_k: weight of the kth Gauss point

$\tilde{I}$: numerical integral

$$\tilde{I} = \sum_{k=1}^{\mathrm{NPG}} p_k\, g(x_k, y_k) \approx \iint_R g(x,y)\, dx\, dy$$

$$= [\mathrm{Jacobian}(T_l)]^{-1} \cdot \iint_{\Omega_l} f(\lambda,\varphi)\, d\lambda\, d\varphi = I, \quad (43)$$

where $g \circ T^l(\lambda,\varphi) = g(x,y) = f(\lambda,\varphi)$.

Applying Eq. (43) to Eq. (42) yields

$$\tilde{a}_{n,m} = \sum_{\Omega_l \in (\Lambda_n \cap \Lambda_m)} \left[\mathrm{Jacobian}(T_l) \times \sum_{k=1}^{\mathrm{NPG}} p_k A(\lambda_k, \varphi_k) \times \cos\varphi_k \left.\frac{\partial P_{i(m,l)}}{\partial\varphi}\right|_{(\lambda_k,\varphi_k)} \left.\frac{\partial P_{i(n,l)}}{\partial\varphi}\right|_{(\lambda_k,\varphi_k)} \right].$$

Applying Eq. (43) similarly to the other coefficients, the actual numerical linear problem must be written

$$[-\tilde{t}_{n,m} + \tilde{a}_{n,m} + \tilde{b}_{n,m} - \tilde{c}_{n,m} - \tilde{d}_{n,m}][\alpha_n] = \left[\frac{a}{g}(\tilde{e}_n + \tilde{g}_n)\right].$$

The accuracy of the numerical integration depends on NPG and on the complexity in space of the integrated quantities. But on the other hand, the numerical cost, in terms of CPU time, of computing the coefficients of the linear system increases linearly with NPG. In Table I, some particular examples are shown. It can be seen that the total degree m increases more slowly than the corresponding number of Gauss points. Some precision tests on a domain where the bathymetry is very regular in space have shown that seven Gauss points are sufficient in a Lagrange-P2 simulation (cf. Le Provost and Vincent [11]).

REFERENCES

1. P. L. Woodworth, *ESA SP* 244, p. 95 (1985).
2. C. Le Provost and A. Poncet, *Int. J. Numer. Methods Eng.* **12**, 853 (1978).
3. C. Le Provost, A. Poncet, and G. Rougier, *J. Phys. Oceanogr.* **11** (8), 1124 (1981).
4. P. Vincent and C. Le Provost, *J. Geophys. Res.* **93** (C1), 543 (1988).
5. E. W. Schwiderski, *Mar. Geod.* **3**, 161 (1980).
6. E. W. Schwiderski, *Mar. Geod.* **3**, 219 (1980).
7. D. E. Cartwright and R. D. Ray, *J. Geophys. Res.* **96** (C3), 3069 (1991).
8. M. L. Genco, Thèse, Université Joseph Fourier, Grenoble I, 1993 (unpublished).
9. F. Lyard, Thèse, Université Joseph Fourier, Grenoble I, 1992 (unpublished).
10. P. Canceill, Thèse, Université Paul Sabatier, Toulouse, 1993 (unpublished).
11. C. Le Provost and P. Vincent, *J. Comput. Phys.* **65** (2), 273 (1986).
12. D. R. Lynch, *Appl. Numer. Methods* **1**, 153 (1985).
13. R. L. Kolar, J. J. Westerink, M. E. Cantekin, and C. A. Blain, *Comput. & Fluids* **23** (3), 523 (1994).
14. J. L. Lions, *Optimal Control of Systems Governed by Partial Differential Equations* (Springer-Verlag, Berlin, 1971).
15. D. R. Lynch, *Oceans 81*, Vol 2 (IEEE, New York, 1981), p 810
16. D. R. Lynch and W. G. Gray, *Comput. & Fluids* 7, 20 (1979).
17. R. F. Henry and R. A. Walters, *Numer. Methods Eng.* **9**, 555 (1993).
18. G. W. Platzman, *J. Phys. Oceanogr.* **8**, 323 (1978).
19. *NOAA NGDC Data Announcement* 88-MG-02: *Digital Relief of the*

Surface of the Eearth (U.S. Department of Commerce, NOAA, NGDC, Boulder, CO, 1988).

20. R. A. Flather, in *Proceedings, Norwegian Coastal Current Symposium, Geilo, Norway, 1980.*
21. W. C. Thacker and R. B. Long, *J. Geophys. Res.* **93**, 1227 (1988).
22. A. Tarantolla and B. Valette, *Rev. Geophys. Space Phys.* **20**, 219 (1982).
23. P. C. McIntosh and A. F. Bennett, *J. Phys. Oceanogr.* **14**, 601 (1984).
24. A. F. Bennett and P. C. Mcintosh, *J. Phys. Oceanogr.* **12**, 1004 (1982).
25. F. Jourdin, Thèse, Université Paul Sabatier, Toulouse, 1992 (unpublished).
26. E. W. Schwiderski, *Mar. Geod.* **6**, 219 (1983).
27. G. Chabert d'Hières and C. Le Provost, *Ann. Hydrograph.* **6**, 5 (1979).
28. D. A. Greenberg, *J. Phys. Oceanogr.* **13** (5) (1983).
29. D. E. Cartwright, B. D. Zettler, and B. V. Hamon, *Pelagic Tidal Constants*, Publ. Sci. Vol. 30, (Int. Assoc. Phys. Sci. of the Oceans, Paris, 1979).
30. D. E. Cartwright and B. D. Zettler, *Pelagic Tidal Constants*, Publ. Sci., Vol. 33 (Int. Assoc. Phys. Sci. of the Oceans, Paris, 1985).
31. M. J. Smithson, *Pelagic Tidal Constants*, Publ. Sci. Vol. 352 (Int. Assoc. Phys. Sci. of the Oceans, Paris, 1992.
32. Internationnal Hydrographic Organisation, Tidal Constituent Bank, Station Catalog, *Ocean and Aquat. Sci.* (Dept. of Fish. and Oceans, Ottawa, 1979).
33. O. Francis and P. Mazzega, *J. Geophys. Res.* **95** (C7), 11, 411 (1990).
34. M. C. Hendershott, *Geophys. J. R. Astr. Soc.* **29**, 389 (1972).
35. A. Kabbaj and C. Le Provost, *Tellus* **32**, 143 (1980).
36. G. Dhat and G. Touzot, *Une Présentation de la Méthode des Eléments finis*, 2nd ed. (Collection Université de Compiègne, Maloine, Paris, 1984).